CHALMERS

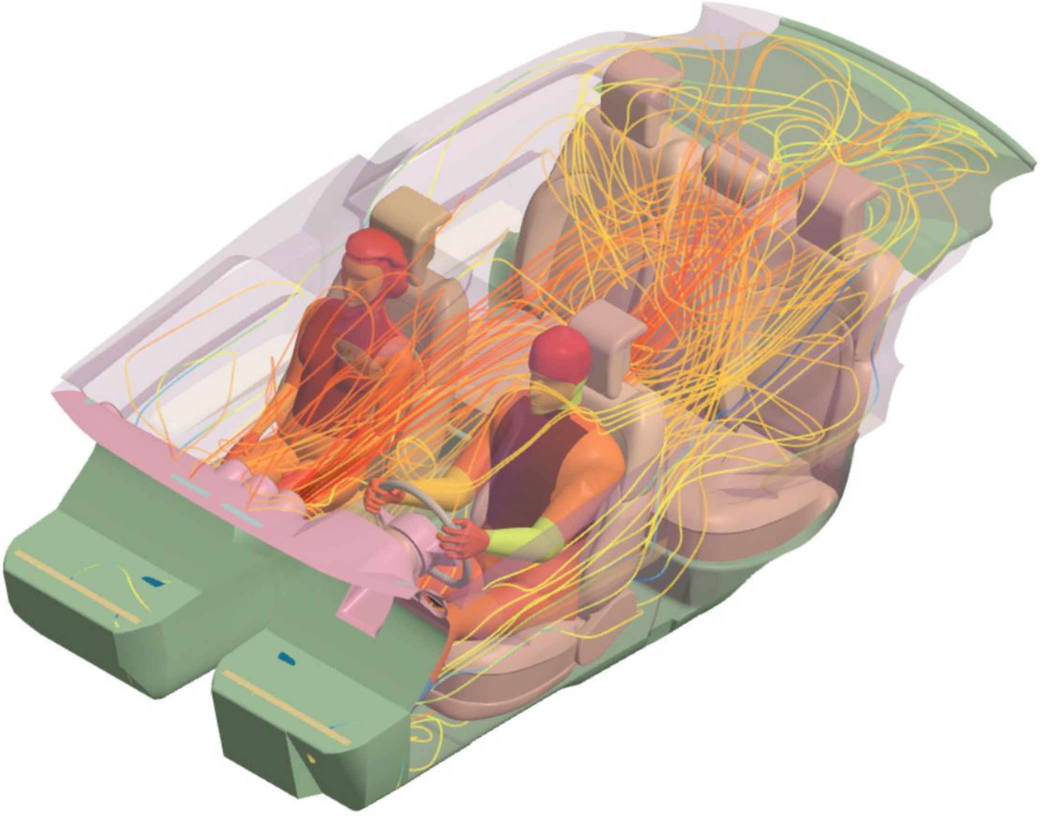

Intelligent Cabins – Energy Efficiency and Passenger Comfort in BEVs

TME180 Automotive Engineering Project 2025

Mohammed Ali El Masri
Rishi Dineshwar
Saeed Al Rahman Chowdhury
Saket Sharad Sapre
Upasana Nandagiri
Vinoth Kanna Chandrasekar

Department of Mechanics and Maritime Sciences
CHALMERS UNIVERSITY OF TECHNOLOGY
Göteborg, Sweden, 2025

Intelligent Cabins – Energy Efficiency and Passenger Comfort in BEVs

TME180 Automotive Engineering Project 2025

Supervisor: Dr. Alexey Vdovin, Department of Mechanics and Maritime Sciences
Supervisor: Prof. Simone Sebben, Department of Mechanics and Maritime Sciences
Examiner: Dr. Alexey Vdovin, Department of Mechanics and Maritime Sciences

Studentarbeten – Mekanik och maritima vetenskaper (M2) – Projektarbete
Department of Mechanics and Maritime Sciences
Chalmers University of Technology
SE-412 96 Göteborg
Sweden
Telephone +46 (0)31 772 1000

Intelligent Cabins – Energy Efficiency and Passenger Comfort in BEVs
Automotive Engineering Project 2025

MOHAMMED ALI EL MASRI
RISHI DINESHWAR
SAEED AL RAHMAN CHOWDHURY
SAKET SHARAD SAPRE
UPASANA NANDAGIRI
VINOTH KANNA CHANDRASEKAR

Department of Mechanics and Maritime Sciences
Chalmers University of Technology
SE-412 96 Göteborg

Abstract

This technical report investigates strategies for enhancing energy efficiency and occupant thermal comfort in Battery Electric Vehicle (BEV) cabins during cold climate operations. Using high-fidelity Computational Fluid Dynamics (CFD) in STAR-CCM+, the study characterizes the complex relationship between HVAC parameters, specifically inlet temperature and mass flow rates, and human physiological responses. The research integrates advanced thermo-physiological models, including the Fiala and Berkeley models, to provide a detailed analysis of local thermal sensation and comfort across diverse occupant demographics.

Key findings from the parametric study indicate that a vane inlet temperature of 32 °C, resulting in an average cabin temperature of approximately 24.6 °C, provides the highest thermal comfort for both male and female occupants, achieving a Predicted Percentage of Dissatisfied (PPD) of nearly 5 %. The study demonstrates that while adjustments to the ventilation mass flow rate have a negligible impact on occupant comfort, reducing the flow from 0.2 kg/s to 0.1 kg/s can yield measurable energy savings, potentially extending vehicle range by 3–5 km during winter driving. Additionally, the results highlight the significant influence of solar loads on thermal perception, noting that occupants feel "chilly" at 24 °C when radiative heating is absent. This work serves as a foundation for designing intelligent, occupancy-aware climate control systems that balance passenger well-being with vehicle performance.

Keywords: Battery Electric Vehicles, Cabin Climate Control, Energy Efficiency, Passenger Thermal Comfort, Fiala Model, Berkeley Model, Predicted Mean Vote, Predicted Percentage of Dissatisfied.

Preface

This technical report presents a comprehensive computational study aimed at enhancing energy efficiency and occupant thermal comfort within battery electric vehicle (BEV) cabins during cold climate operation. Utilizing high-fidelity Computational Fluid Dynamics (CFD) in STAR-CCM+, our research characterizes the complex interplay between HVAC parameters, such as inlet temperature and mass flow rates, and human physiological responses. By integrating advanced thermo-physiological models, including the Fiala and Berkeley models, we provide a detailed analysis of local thermal sensation and comfort across diverse occupant demographics. This work serves as a foundation for designing intelligent, occupancy-aware climate control systems that balance passenger well-being with vehicle performance.

Acknowledgment

We would like to express our sincere gratitude to everyone who contributed to the successful completion of this project, whether through direct involvement or indirect support.

First and foremost, we extend our heartfelt thanks to our supervisor and examiner, Alexey Vdovin. We are deeply grateful for his unwavering support and for the wisdom he shared from his extensive experience in the field. His guidance was instrumental in shaping our work, and the essential computational resources he provided were vital in ensuring the project was completed within the established time frame.

We also wish to convey our sincere appreciation to our co-supervisor, Professor Simone Sebben. Her invaluable insights and consistent guidance ensured the technical integrity of our research and kept the project on the right path.

Finally, we would like to thank Chalmers University of Technology for providing the necessary software licenses and access to institutional resources, which were fundamental to our technical analysis and overall project execution.

Declaration on the use of ‘Artificial Intelligence’

We declare hereby that the usage of generative ‘Artificial Intelligence’ tools within the scope of this project was limited to basic numerical calculations, summarizing research articles, LaTeX report suggestions or corrections, and comprehension of some concepts. The project group reviewed the project and takes full responsibility for its contents.

Nomenclature

List of Abbreviations

BEV	Battery Electric Vehicles
CAD	Computer-Aided Design
CFD	Computational Fluid Dynamics
DTS	Dynamic Thermal Sensation
HVAC	Heating, Ventilation and Air Conditioning
ICE	Internal Combustion Engines
PMV	Predicted Mean Vote
PPD	Predicted Percentage of Dissatisfied
PTC	Positive Temperature Coefficient
S2S	Surface-to-Surface
TE	Thermoelectric

List of Symbols

$\bar{t}_r$	Mean radiant temperature (°C)
$\dot{m}$	Mass flow rate (kg/s)
λ	Thermal conductivity (W/m·K)
μ	Dynamic viscosity (Pa·s)
∇	Gradient (Nabla) operator
ρ	Fluid density (kg/m^3)
$\vec{v}$	Velocity vector (m/s)
A	Cross-sectional area (m^2)
c_p	Specific heat at constant pressure (J/kg·K)
F_z	Volume forces (N)
f_{cl}	Clothing surface area factor
h_c	Convective heat-transfer coefficient (W/m^{2}K)
I_{cl}	Clothing insulation (m^{2}K/W)
M	Metabolic rate (W/m^2)

p	Static pressure (Pa)
p_a	Water vapor partial pressure (Pa)
T	Temperature (°C)
t	Time (s)
t_a	Air temperature (°C)
t_{cl}	Clothing surface temperature (°C)
u, v, w	Velocity components in x, y, z directions (m/s)
v_{ar}	Relative air velocity (m/s)
W	Mechanical power (W/m^2)
y^+	Dimensionless wall distance

Contents

List of Figures

List of Tables

1 Introduction

The ongoing transition from conventional ICEs to BEVs introduces a significant challenge regarding cabin climate control. In traditional ICE vehicles, the engine generates substantial waste heat during combustion, which is absorbed by the liquid cooling system. This thermal energy is diverted to a heater core within the HVAC system, providing "free" cabin heating with negligible impact on fuel economy.

In contrast, battery electric vehicles lack a high-grade thermal waste source. Although electric motors, power electronics, and auxiliary components generate heat, the available thermal energy is marginal compared to internal combustion engines and is generally insufficient for cabin heating in cold climates. In addition, batteries must be maintained within a narrow temperature range to ensure efficient operation and to reduce safety risks. As a result, cabin heating in battery electric vehicles is typically provided by high-voltage electric heaters or heat pump systems, both of which draw energy directly from the traction battery.

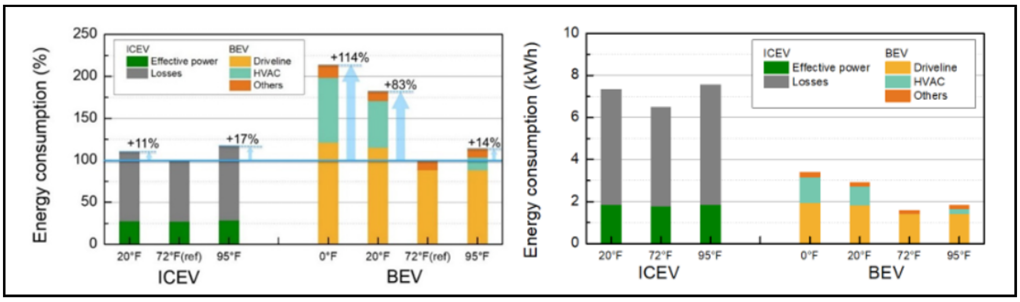

Figure 1: Effect of ambient temperature on the energy consumption of ICEs compared with BEVs [1]

As illustrated in Figure 1, the energy consumption of a BEV increases significantly as ambient temperatures decrease. Specifically, the HVAC energy demand exhibits an exponential growth trend as the thermal gradient between the cabin setpoint and the exterior environment widens. This consumption pattern is a critical factor in vehicle performance; every unit of energy diverted to the HVAC system directly reduces the available driving range. Given the decisive impact of ambient temperature on battery state-of-charge, there is an urgent need to develop energy-efficient thermal management strategies to optimize battery utilization, extend range, and mitigate consumer range anxiety.

Consequently, optimal climate control strategies are essential to minimize battery energy consumption while fulfilling the primary objective of the HVAC system: maintaining the thermal comfort of cabin occupants. This theoretical study focuses on evaluating the influential factors of the HVAC system that govern human thermal perception.

The investigation begins with a foundational overview of the physical principles used to assess human thermal comfort via computational simulations. Subsequently, a comprehensive methodology and workflow were established to execute the study. The technical approach was divided into the following phases:

Flow Characterization: Initially, a cold flow simulation was conducted to establish a baseline understanding of the aerodynamic characteristics within the cabin volume.

Grid Convergence: A mesh independence study was performed to evaluate various discretization levels, balancing numerical accuracy with available computational time and resources.

Parametric Analysis: A suite of simulations was executed to investigate specific HVAC parameters hypothesized to impact occupant comfort.

Optimization and Strategy: Following post-processing of the simulation data, intelligent control strategies were formulated.

1.1 Aim

The aim of this project is to study the factors that affect the thermal comfort and thermal sensation of occupants in a cold climate, and to assess strategies that can improve both passenger comfort and energy consumption in battery electric vehicles

To achieve this aim, the project has the following objectives:

- To build a CFD model of a BEV cabin, including human occupants, and to identify an optimal temperature range that provides good comfort for both male and female manikins.
- To perform a parametric study by varying vane inlet temperature, mass flow rate, and the impact of solar loads, and evaluate their effect on comfort through indices such as PMV and PPD.
- To discuss energy-efficient strategies that could be applied in real vehicles, such that they could improve the thermal comfort of the occupants while reducing energy consumption.[2]

1.2 Boundaries

Key limitations and constraints need to be established to ensure the project remains focused and feasible.

- The scope has been constrained only to battery electric passenger vehicles.
- The simulation domain will be focused on the cabin and its effects, but not the influence on the entire vehicle's performance characteristics.
- The work is conducted as a purely theoretical study, including literature review, meshing, and simulations, and does not include any validation with physical or experimental data.
- The project will take into account the restrictions that the time frame and available computing resources have on it.

2 Theoretical background

This chapter gives a brief introduction to the theory used as the basis of this project, namely fluid mechanics and mathematical models for thermal comfort.

2.1 Governing Equations

Governing equations describe the fundamental conservation laws of mass, momentum, and energy that must be satisfied in fluid flow simulations. These equations form the basis of numerical fluid mechanics and ensure that physical quantities are conserved within a control volume. In practical terms, they relate the temporal change of a quantity inside a system to the net flux entering or leaving the system.

2.1.1 Conservation of Mass (Continuity Equation)

According to classical mechanics, the mass going through the system cannot disappear; it should either come out of the system or increase the mass of the system. The law of conservation of mass can be mathematically defined as follows

$$\dot{m} = \rho \cdot A \cdot v \quad \text{, where A is the area and v is the velocity} \tag{1}$$

In words, the temporal change of mass corresponds to the flow of mass in and out through the area with a velocity.

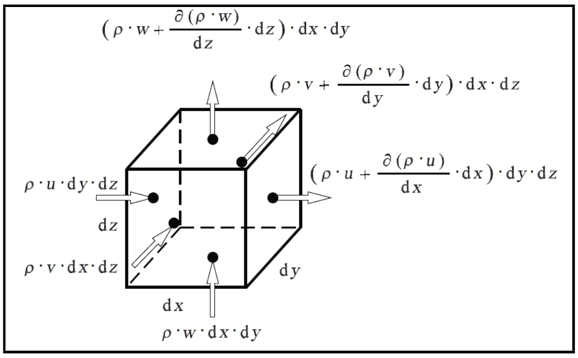

Figure 2: In and out-flowing mass flux in a control volume [3]

A simplified continuity equation without extensive derivation is given by,

$$\frac{\partial \rho}{\partial t} + \frac{\partial (\rho \cdot \mathrm{u})}{\partial x} + \frac{\partial (\rho \cdot \mathrm{v})}{\partial z} + \frac{\partial (\rho \cdot \mathrm{w})}{\partial y} = 0 \tag{2}$$

And in coordinate-free notation, it can be written as

$$\frac{\partial \rho}{\partial t} + \nabla \cdot (\rho . \vec{v}) = 0 \text{ or for incompressible flows } \nabla \cdot \vec{v} = 0$$

2.1.2 Conservation of Momentum (Navier-Stokes Equation)

Analogous to mass flow, momentum is also a conservation quantity and can be determined in a similar way. Momentum, as in classical Newtonian mechanics, can be defined as the product of mass and velocity. Momentum flow, on the other hand, is the flow of momentum through an area with velocity v. In the same way as conservation of mass, the temporal change of the momentum in the control volume is the difference between the sum of momentum flow through, and the sum of momentum flow out of the control volume.

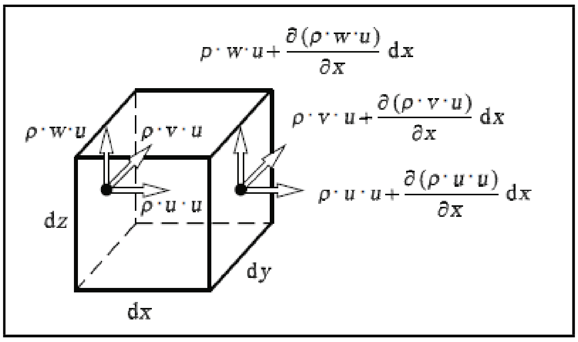

Figure 3: In and out-flowing momentum flux in a control volume in x direction [3]

Taking a balance of the temporal change of the momentum, normal, and shear stress for each direction component, neglecting other field forces like gravity, magnetism, or inertial forces in relative systems, and simplifying using substitution and resolving for normal and shear stress in all three dimensions, we get a set of equations popularly known as the Navier-Stokes equations.

$$\underbrace{\rho\left(\frac{\partial u}{\partial t}+(u\cdot\nabla)u\right)}_{\text{acceleration forces (inertia)}} = \underbrace{F_z}_{\text{volume forces}} - \underbrace{\nabla p}_{\text{pressure forces}} + \underbrace{\mu\nabla^2 u}_{\text{shear stress forces (viscous forces)}}$$

2.1.3 Conservation of Energy

Since the scope of the project deals with heat transfer, it is important to consider the conservation of energy as well. It can be defined as the temporal change in the inner energy and the kinetic energy of the gases, which in turn is basically a summation of energy due to pressure, viscous dissipation, thermal conduction (Fourier diffusion), and energy from a heat source. [3] The equation can be mathematically written in the following form

$$\underbrace{\rho c_p \frac{\partial T}{\partial t}}_{\text{Transient thermal energy storage}} + \underbrace{\rho c_p (u\cdot\nabla T)}_{\text{Convective heat transport}} =$$

$$\underbrace{\left(\frac{\partial p}{\partial t}+u\cdot\nabla p\right)}_{\text{Pressure work}} + \underbrace{\nabla\cdot(\lambda\nabla T)}_{\text{Thermal conduction}} + \underbrace{\rho\dot{q}_s}_{\text{Heat source}} + \underbrace{\mu\Phi}_{\text{viscous dissipation}}$$

The scope of this work lets us make some assumptions and apply them to the above equation, such as:

- the velocity is low and viscous dissipation is negligible
- the fluid is incompressible.

Therefore, the above equation can be simplified in the following way:

$$\rho c_p \left(\frac{\partial T}{\partial t} + u \cdot \nabla T \right) = \nabla \cdot (\lambda \nabla T) + \rho \dot{q_s}$$

2.2 Human Thermal Comfort and Comfort Models in Star-CCM+

Thermal comfort refers to a condition of mind in which a person experiences satisfaction with the thermal environment. It is achieved when the body's heat production and heat loss are in equilibrium, maintaining the internal body temperature within a narrow range. In vehicle cabins, achieving thermal comfort is particularly challenging because the thermal environment is non-uniform and transient, with strong gradients in air temperature, velocity, and radiation between different body regions. These challenges have led to the development of several thermal comfort models, from classical steady-state approaches to more advanced physiological models, which are reviewed in this section.

2.2.1 Predicted Mean Vote (PMV)

The predicted mean vote is an empirical model developed by Fanger in the 1960s to quantify thermal comfort by relating physiological heat balance to subjective thermal sensation. The predicted mean vote is a thermal comfort index that estimates the average thermal sensation of a large group of occupants exposed to a given environment. Its formulation is standardized in international guidelines such as ISO 7730 and ASHRAE 55.

$$PMV = (0.303e^{(-0.036M)} + 0.028)L$$

, where M is the metabolic rate in W/m^2 and L is the difference between internal heat production and heat loss under given conditions [4].

The PMV equation with thermal load L, which takes the environmental and clothing influence into consideration, can be commonly expanded as,

$$\begin{aligned} \text{PMV} = \; & [0.303 \exp(-0.036M) + 0.028] \times \Bigg\{ (M - W) - 3.05 \times 10^{-3} \\ & [5733 - 6.99(M - W) - p_a] - 0.42\,[(M - W) - 58.15] \\ & - 1.7 \times 10^{-5} M (5867 - p_a) - 0.0014 M (34 - t_a) \\ & - 3.96 \times 10^{-8} f_{cl} \left[(t_{cl} + 273)^4 - (t_r + 273)^4 \right] - f_{cl} h_c (t_{cl} - t_a) \Bigg\} \end{aligned}$$

It uses a 7-point scale ranging from. -3 (Very Cold) to +3 (Very Hot), with 0 showcasing thermal neutrality. Of the above-mentioned variables, there are six key factors in the PMV index: air temperature, mean radiant temperature, relative humidity (contained within water vapor partial pressure), air velocity, metabolic rate, and clothing insulation. The original model was limited to steady-state, air-conditioned, moderate climates, yet it is of much importance as it has been adopted by multiple international standards [6].

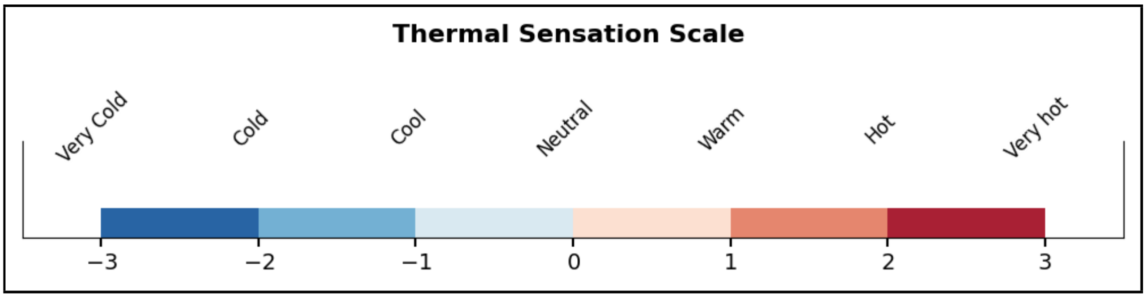

Figure 4: Thermal sensation spectrum

2.2.2 Predicted Percentage of Dissatisfied (PPD)

The PPD is an empirical curve fit linked to Fanger's PMV to observe the fraction of subjects who reported being clearly too hot or too cold (votes $\leq$-2 and $\geq$+2). The relation between PPD and PMV is given in [4] by

$$PPD = 100 - 95\exp(-0.03353PMV^4 - 0.2179PMV^2)$$

From the equation, it is evident that the percentage of people likely to be dissatisfied even at a PMV of 0 (thermal neutrality) is at least 5%. As PMV moves away from 0, the PPD rapidly increases. International Standards such as ISO7730 and ASHRAE55 recommend maintaining PMV between -0.5 to +0.5, which typically corresponds to having a PPD less than 10% for acceptable thermal comfort levels. [7]

2.2.3 Fiala Model

The Fiala model is a detailed thermo-physiological model that predicts the human body's thermal response by simulating heat transfer within and between body tissues. It divides the human body into multiple segments (head, torso, limbs) and layers (core, muscle, fat, skin), and it includes regulatory mechanisms such as sweating, shivering, vasodilation, and vasoconstriction. The model computes both transient core and skin temperatures as the body interacts with its environment.

Within STAR-CCM+, the Fiala model is dynamically coupled with the CFD solver: local air temperature, velocity, evaporation of moisture from the skin, and radiation values from the CFD simulation are passed to the model, which returns segmental skin temperatures and heat fluxes. This enables transient comfort evaluations of how quickly a passenger transitions from cold to comfortable or begins to feel hot when cooling is reduced. The Fiala model provides the physiological foundation, while the Berkeley model interprets the resulting thermal sensation. Used together, they allow a complete assessment of both the physical and subjective aspects of thermal comfort.

In STAR-CCM+, the Fiala Thermal comfort model requires the human manikin to be divided into 58 body parts [8], as shown in Figure 5. Each part represents an individual thermal zone where local heat transfer is calculated based on the surrounding air temperature, radiation, and convection. This segmentation allows the model to capture asymmetrical comfort conditions, such as when the face is warm while the feet are cold, by computing local thermal sensations for each region. The local results are then combined into overall comfort indices such as the Dynamic Thermal Sensation (DTS) and the PPD.

Figure 5: 58 surfaces as required by the Fiala thermal model

2.2.4 Berkeley Model

The Berkeley model, developed at the Center for the Built Environment (University of California, Berkeley), predicts human thermal sensation and comfort using a segment-based approach. It divides the human body into multiple regions and calculates local thermal sensation votes based on the environmental conditions experienced by each region. The model translates local skin temperatures and their rates of change into subjective sensation levels (cold–hot) and combines them into an overall comfort index.

Local thermal sensation and comfort are assessed for 19 body segments (Figure 6), including the head, face, breath, neck, chest, back, pelvis, left and right upper arms, left and right lower arms, left and right hands, left and right thighs, left and right lower legs, and left and right feet. Local thermal sensation is dependent on the local skin temperature as well as the mean skin or core body temperature. Local thermal comfort is determined by a combination of local thermal sensation and overall whole-body sensation.[8]

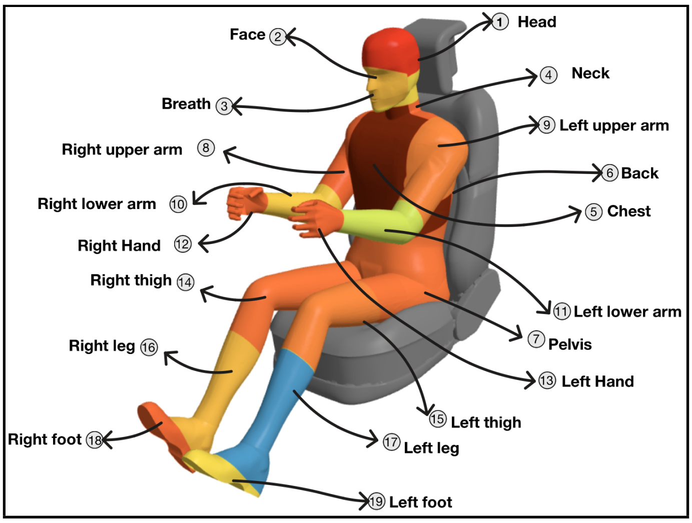

Figure 6: 19 Segments as required by the Berkeley thermal model

2.2.5 Role of Clothing and Metabolism

Metabolic heat generation and clothing strongly influence thermal comfort but are not explicitly simulated in STAR-CCM+. Instead, they are specified as boundary conditions for the human model. The *metabolic rate* (in MET units) determines the internal heat production, while the *Clothing evaporative resistance* controls the heat resistance between the skin and the air. According to ISO 9920 [9], typical clothing ensembles range from 6 to 20 Pa m^2/K (typical summer clothing) and 50 to 100+ Pa m^2/K (winter wear). These parameters should be defined based on experimental or standard data to ensure realistic results.

Clothing materials influence both heat and moisture transport. Pan et al.[10] emphasize that the structure and fiber composition of clothing significantly affect its thermal insulation and vapor resistance. Similarly, Khatoon et al.[11] demonstrated that both clothing and metabolic factors alter the equivalent ambient temperature (EAT) perceived by passengers, and must be considered when evaluating comfort. Thus, while STAR-CCM+ does not model clothing layers explicitly, accurate assignment of clothing and activity parameters to the corresponding segments remains essential for realistic comfort predictions.

3 Methodology

This section details the numerical framework established to evaluate thermal comfort within the BEV cabin. The methodology was executed in a sequential workflow: defining the cabin geometry and occupants, establishing mesh independence, validating the aerodynamics via cold flow simulations, and finally conducting a comprehensive parametric study. The entire methodology is visualized in the form of a tree diagram in Figure **??**.

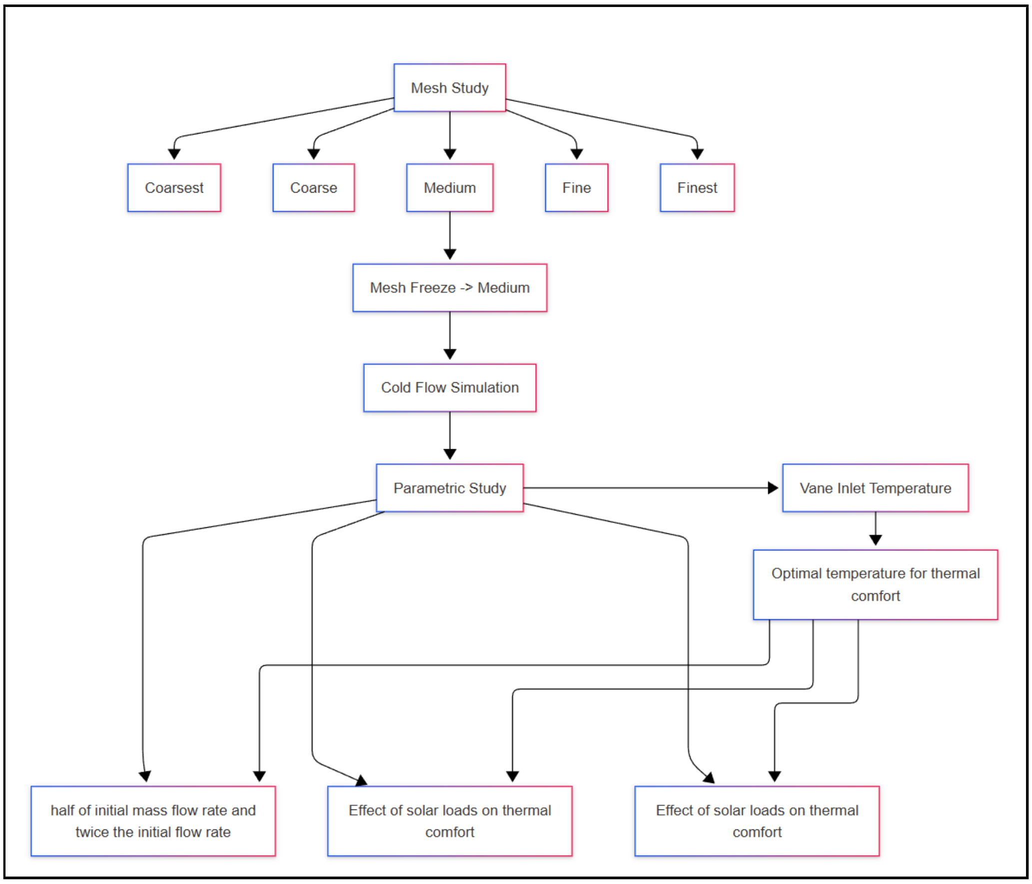

Figure 7: Applied workflow

This structured workflow ensures numerical reliability by first validating airflow behavior and mesh independence before introducing thermal comfort models and parametric variations. Such a staged approach minimizes numerical uncertainty and allows clear attribution of comfort outcomes to specific HVAC parameters.

3.1 Cabin Geometry and Computational Domain

The computational domain represents a generic sedan-style cabin. The geometry for the cabin structure was adopted from the standard STAR-CCM+ thermal comfort tutorial, which is shown in Figure 8. While the cabin geometry is generic, it retains all dominant internal flow obstacles to ensure realistic airflow distribution and recirculation patterns.

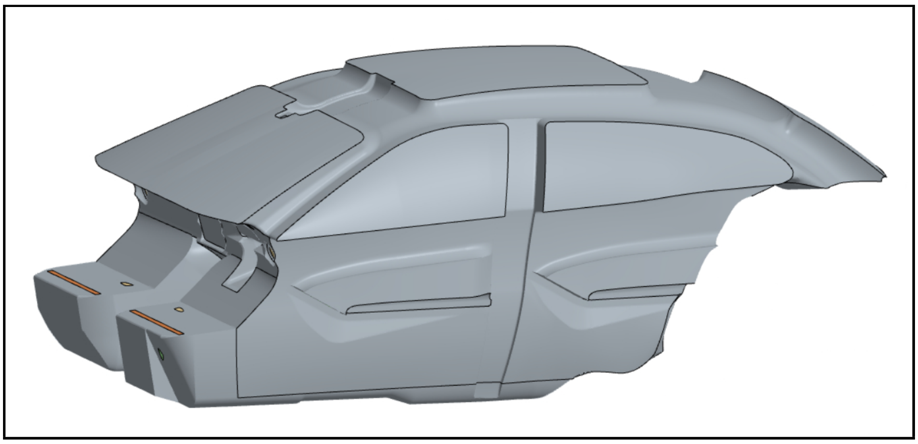

Figure 8: External view of the cabin geometry

To focus specifically on internal thermal comfort, the exterior or aerodynamic part of the passenger car was excluded. Instead, the cabin was treated as an enclosed fluid volume bounded by thermally active solid shells (glass, roof, doors, and floor), which are made transparent in the figure 9. The fluid domain includes the main cabin air volume and internal solid structures such as the dashboard, front seats, rear bench, and center console (surfaces represented in pink in the Figure 9), which were retained as obstacles to accurately capture flow recirculation and blockage effects.

Special attention was given to the ventilation system, which includes five distinct vent groups modeled to represent a standard heating distribution:

- **Defrost Vents:** Located at the base of the windshield.
- **Front Main Vents:** Adjustable vanes on the dashboard.
- **Front Floor Vents:** Directed towards the driver and passenger feet.
- **Rear Center Console Vents:** Delivering air to the rear passengers.
- **Rear Floor Vents:** Located beneath the front seats.

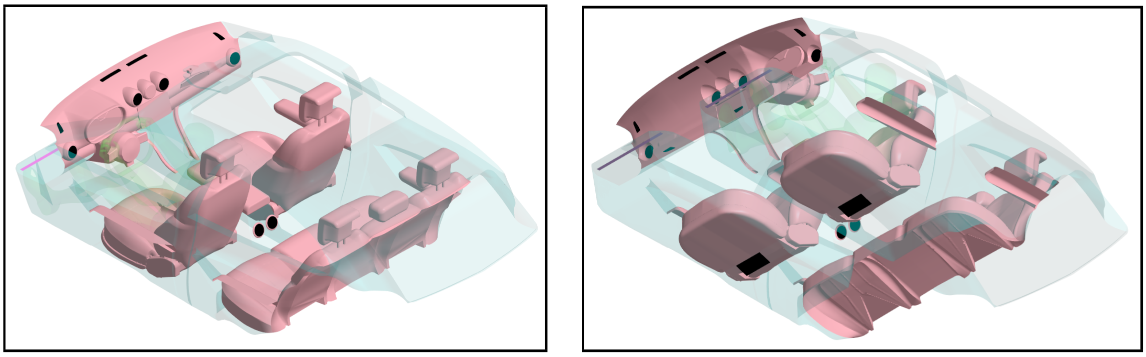

Figure 9: Inlet vents (surfaces are represented in black)

3.2 Manikin Modeling and Preparation

Human occupants act as both heat sources and thermal sensors within the simulation. To capture realistic blockage and heat generation, virtual manikins were utilized in the driver and passenger seats.

Manikin Generation and Positioning

The occupant setup involved a hybrid approach utilizing both pre-configured assets and custom-generated models:

1. **Baseline Male Driver:** The driver seat was occupied by the pre-configured 50th percentile male manikin (Figure 10) provided within the STAR-CCM+ tutorial assets (Height: $1.76m$, Weight: $77kg$). This was used as a baseline to understand the workflow, boundary conditions, and thermal comfort modeling approach.

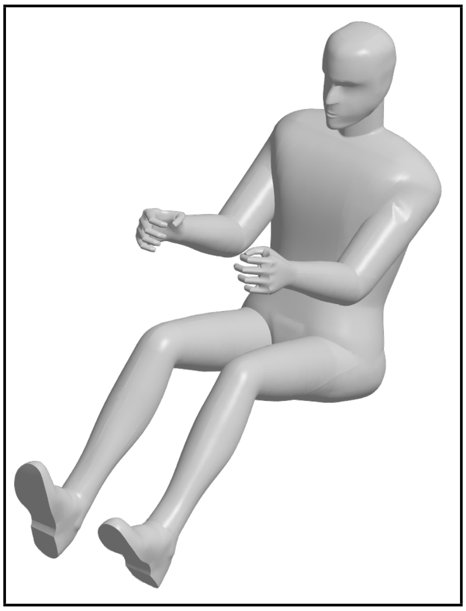

Figure 10: Male driver manikin

2. **Custom Manikin Setup:** The male driver manikin provided in the tutorial was already a fully meshed entity with a fixed posture. Due to this, it could not be repositioned or modified to represent a passenger. Therefore, to expand the study to different demographics and occupancies, three additional manikins (Female Driver, Male Passenger, Female Passenger) were introduced.

The manikins were created using surface-based human models (Figure 11) provided by Professor Håkan Almius, Department of Industrial and Materials Science, Chalmers University of Technology. These models were editable surface geometries, allowing posture adjustment and positioning inside the cabin prior to meshing. The manikins were positioned in both driver and passenger seating locations to represent realistic occupant postures (Figure ??). This ensured correct alignment with the seats and cabin layout before further processing.

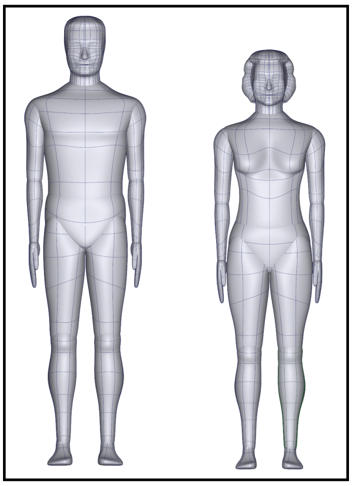

Figure 11: Surface-based human manikins

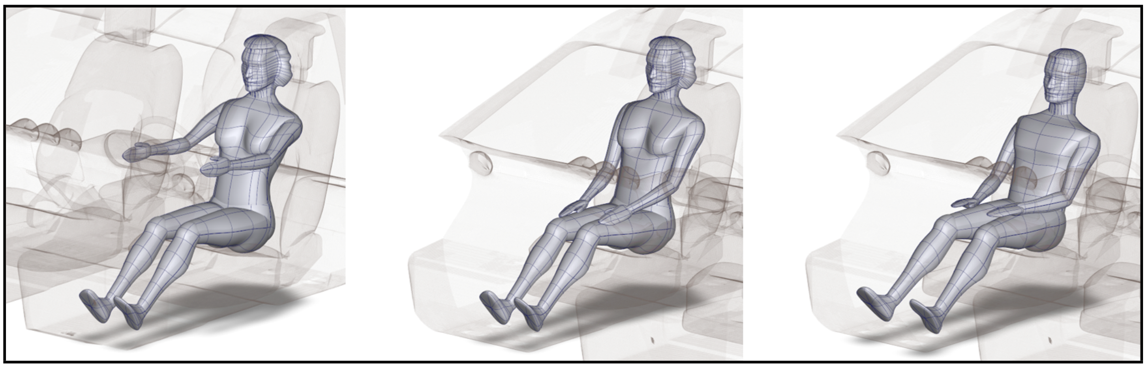

Figure 12: Manikins positioned in driver and passenger locations inside the cabin

Surface Segmentation for Comfort Models

To interface correctly with the thermal comfort solvers, the manikin geometry required specific surface splitting. The alias surface-based manikins were segmented into multiple body regions using cutting planes (Figure 13). This segmentation follows the requirements of the STAR-CCM+ thermal comfort models, which evaluate heat transfer and comfort on a body-part basis rather than as a single averaged value. The female manikin was prepared for driver and passenger positions, whereas the male manikin was prepared for the passenger position. An example of only the female model post-segmentation is represented in Figure 13.

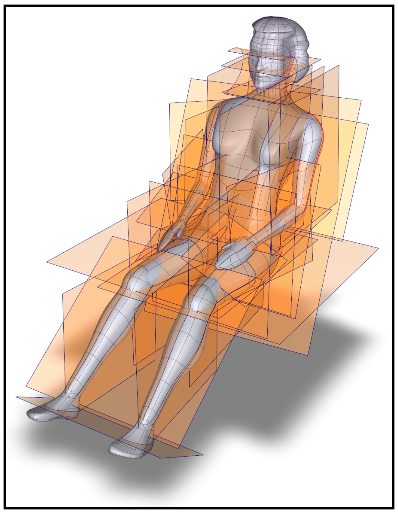

Figure 13: Manikin segmented using planes

After splitting the manikin, the manikin's surfaces were verified to have 58 distinct thermal segments (e.g., forehead, chest, upper arm, thigh, calf, foot). This granular segmentation is essential for the Fiala model to calculate local heat transfer coefficients (h) and skin temperatures (T_{skin}) specific to different body parts.

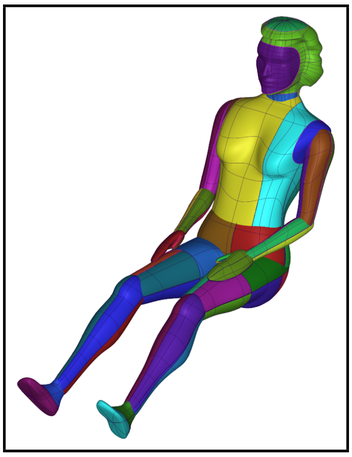

Figure 14: The segmented manikin geometry showing the 58 distinct thermal regions used for the Fiala model

Secondly, for the evaluation of thermal sensation, these 58 physiological patches were mapped to the 19 key segments defined by the Berkeley Comfort Model. This grouping allows the simulation to aggregate physical data into psychological sensation scores (e.g., "Slightly Warm" or "Cold") for major body parts. The 19 segments and their numbering are shown in Figure 15.

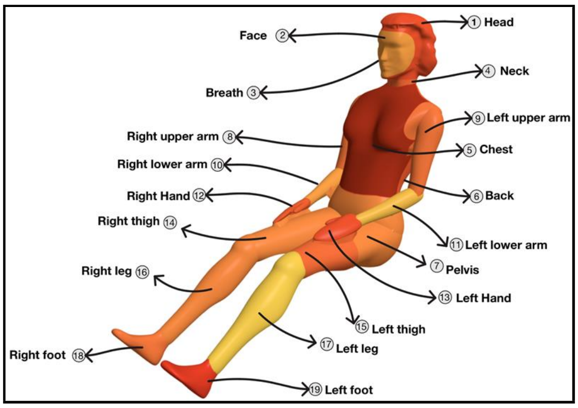

Figure 15: Representation of the 19 Berkeley segments used for the evaluation of local thermal sensation and comfort

Clothing Resistance

To simulate the thermal resistance provided by apparel, clothing resistance values were applied directly to the manikin boundaries. Instead of modeling the physical geometry of the clothes, a thermal resistance boundary condition was mapped to the specific surface segments.

For this study, a standardized light clothing ensemble was defined for all occupants, consisting of a shirt, shorts, and shoes. The clothing evaporative resistance and contact resistance were assigned to the corresponding anatomical segments as detailed in Table 1. Exposed skin areas such as the face and hands were assigned a value of 0 Pa m^2/W to allow for direct convective exchange.

Table 1: Clothing insulation values applied to specific manikin segments

Body Segment	Clothing Item	Clothing evaporative resistance	Contact resistance
Torso & Arms	Shirt (Short Sleeve)	6.5 Pa m^2/W	0.077 m^2K/W
Pelvis & Thighs	Shorts	18.2 Pa m^2/W	0.096 m^2K/W
Feet	Shoes & Socks	6 Pa m^2/W	0.062 m^2K/W
Other segments	Exposed Skin	0 Pa m^2/W	0 m^2K/W

Physiological Differences

A key contribution of this study is the differentiation between male and female physiology. Standard automotive testing often relies solely on the male manikin, which can lead to climate control systems that are suboptimal for female occupants. Literature indicates that females generally possess lower metabolic rates and lower mean skin temperatures than males under identical environmental conditions [12]. To reflect this, the simulation parameters were customized as shown in Table 2.

Table 2: Physiological parameters defined for the male and female manikins

Parameter	**Male Manikin**	**Female Manikin**
Percentile	90th	5th
Metabolic Rate (Driving)	1.0 MET	≈ 0.9 MET
Target Mean Skin Temp.	34.0 °C	33.0 °C
Surface Area	1.9 m^2	1.5 m^2

Selecting the 5th percentile female and 95th percentile male manikins is a standardized "design for extremes" approach that ensures the vehicle cabin accommodates the vast majority of the population. Specifically, the 95th percentile male model serves as the upper boundary, representing an individual who is larger than 95% of the male population. Conversely, the 5th percentile female model represents the lower boundary, as only 5% of the female population is smaller in stature. By testing these two boundary models, engineers can statistically verify that approximately 90% to 95% of the mixed-gender population—including those of "average" size who fall between these extremes—will experience adequate thermal comfort and ergonomic fit. This methodology is particularly critical in thermal evaluation because it accounts for the diverse physiological responses of both small and large occupants.

3.3 Cold Flow Simulation

Since the cold flow simulation is performed solely to analyze the fluid behavior, the setup was intended to be as simple as possible. This preliminary study was conducted on an empty cabin configuration (no driver or passengers) under the steady state assumption. To optimize computational resources without compromising the resolution of the flow field, a medium-density mesh was implemented. Inlets with a mass flow rate of 0.04 kg/s, outlets as a pressure outlet, and all the surfaces as static walls served as the boundary conditions.

To assess the flow field, velocity magnitude was analyzed on a longitudinal plane cutting vertically through the driver's seating position, as seen in Figure 16. The specific physical models used to characterize the internal airflow are listed in Table 3.

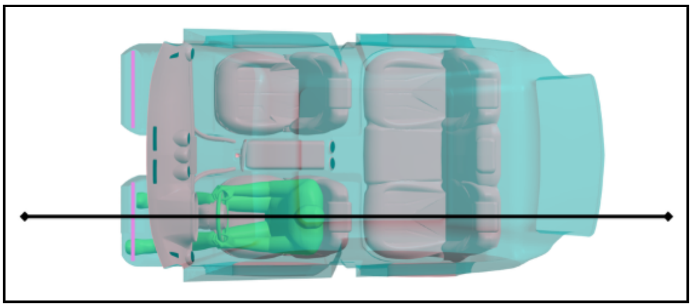

Figure 16: Position of the longitudinal plane section passing through the driver seat used for velocity analysis

Table 3: Physics solvers and models enabled for the cold flow simulation

Category	**Selected Model**
Material	Gas (Constant Density)
Flow Solver	Segregated Flow
Viscous Regime	Turbulent
Turbulence model	Realizable K-Epsilon (Two-layer all y+)
Time Domain	Steady
Dimensionality	Three Dimensional
External Forces	Gravity

This step confirmed that the inlet definitions produced a physically reasonable cabin flow field, identifying recirculation zones without the complexity of heat transfer.

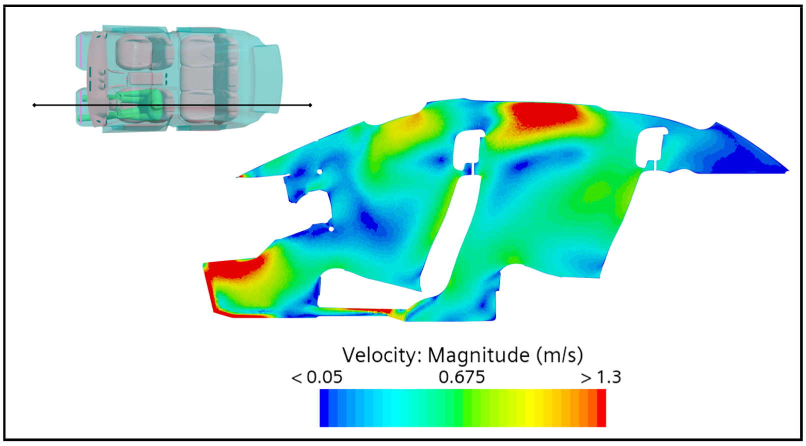

Figure 17: Velocity magnitude distribution on a longitudinal plane section passing through the driver seat

The key observations from the velocity profile are numbered as follows. At Point 1, high air speeds are observed due to the proximity of both an inlet and an outlet vane. Compared to other inlets, the vanes near the feet have a smaller cross-sectional area, which explains these elevated velocities. At Point 2, the high speed is a result of local flow narrowing. Conversely, the high velocity at Point 3 is driven by strong flow from the two central dashboard inlet vanes, which subsequently recirculates toward the rear seats. To visualize this behavior, a streamline plot was generated as shown in figure 18.

The streamlines clearly illustrate the recirculation of air toward the rear passenger seats and its return to the front outlet located near the floor. It is important to note that the flow is primarily directed at the chest and face regions, while there is minimal to no flow near the leg region. Additionally, a "short circuit" of the flow, where air moves directly from the front floor vanes to the outlet, is visible. The consequences of this behavior will be discussed in the upcoming sections.

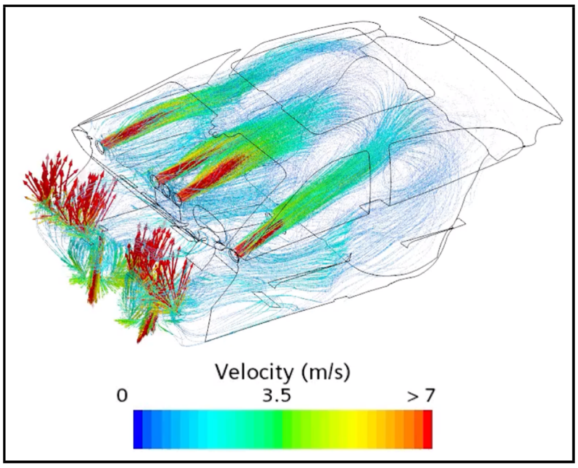

Figure 18: Streamline plot of the velocity profile

3.4 Mesh Study

To ensure that the simulation results were independent of the grid resolution, a mesh sensitivity analysis was conducted. The objective was to determine the optimal cell count that balances computational efficiency with numerical accuracy, ensuring that further refinement of the mesh would not significantly alter the flow or thermal solution.

Mesh Generation and Parameters

The domain was discretized using the Polyhedral mesher in STAR-CCM+, selected for its ability to capture complex cabin geometries with fewer cells compared to tetrahedral meshes. To accurately resolve the boundary layer flow and heat transfer at the walls, Prism Layers were applied to all no-slip surfaces (manikins, dashboard, windows), ensuring a dimensionless wall distance ($y+$) suitable for the turbulence model. The specific boundary conditions applied during this sensitivity analysis are detailed in Table 4.

Table 4: Boundary conditions applied during the mesh sensitivity study

Parameter	**Value**	**Unit**
Inlet Air Temperature	16	°C
Inlet Mass Flow Rate (Entire Cabin)	0.2	kg/s
Exterior Convection Temperature	10	°C
Driver Skin Temperature	34	°C
Thermal Manikin Body Temperature	36.5	°C

Grid Sensitivity Criteria

To identify the optimal grid density, 5 mesh cases were set up. The mesh densities varied from very coarse, coarse, medium, fine, and very fine. The minimum surface sizes and the number of cells for each case are described in Table 5. The motivation was to find a configuration that delivered accurate results while remaining computationally fast, as strict time restraints were a factor in the project timeline. The selection criteria used to judge the trade-off between accuracy and cost:

1. Volume-Averaged Temperature: Employed as a primary metric to identify a grid-independent representation of the thermal field.
2. Total Pressure Drop: Employed as a primary metric to identify a grid-independent representation of the flow field and associated aerodynamic resistance.
3. Computational Time: Considered as an additional criterion to select, among the grid-independent meshes, the configuration with the minimum number of cells that allowed completion of the full parametric study within the project deadlines.

Table 5: Mesh description and cell count

Description	**Minimum Surface Size (mm)**	**No. of Cells**
Very Coarse	5	6 Million
Coarse	4	8 Million
Medium	3	13 Million
Fine	2	24 Million
Very Fine	1.5	36 Million

As the mesh was refined from 6 million to 13 million cells, a noticeable change in the predicted average cabin temperature was observed. However, further refinement beyond 13 million cells resulted in negligible variation in temperature values, as shown in figure 19. Specifically, the average cabin temperature changed from 15.73 °C at 13 million cells to 15.72 °C and 15.70 °C for 24 million and 34 million cells, respectively. This marginal difference indicates that the temperature field had effectively converged at the medium mesh resolution.

A similar trend was observed for the pressure drop between the inlet and outlet vents. The pressure drop decreased significantly when refining the mesh from 6 million to 13 million cells, reducing from 23.1 Pa to 19.5 Pa as depicted in 20. Beyond this point, further mesh refinement led to only minor reductions (18.22 Pa at 24 million cells and 17.7 Pa at 34 million cells), suggesting diminishing returns in solution accuracy.

Based on these observations, the 13-million-cell mesh was deemed sufficient to capture the essential flow and thermal characteristics of the cabin. Further mesh refinement did not yield substantial improvements in accuracy, while significantly increasing computational time and resource requirements. Therefore, the medium mesh (13 million cells) was selected for all subsequent simulations as it provides an optimal compromise between numerical accuracy and computational efficiency.

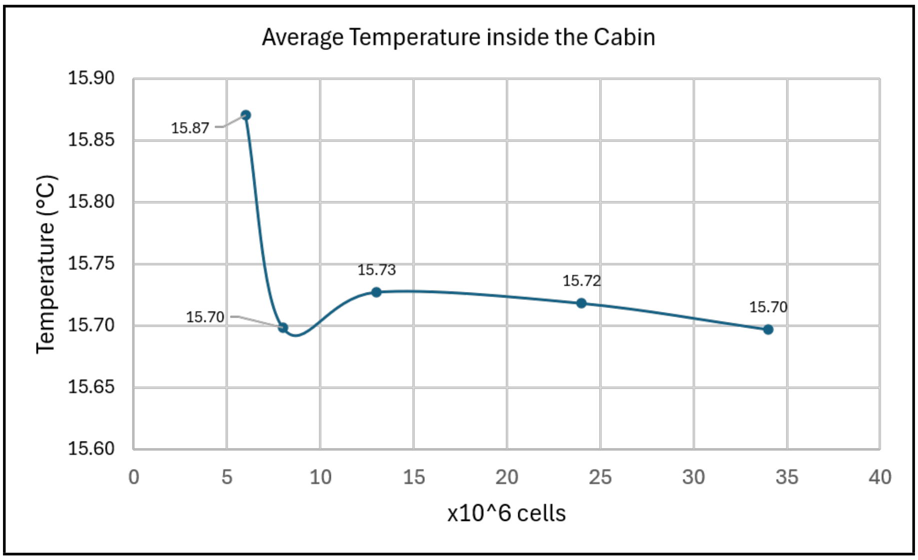

Figure 19: Variation of average cabin temperature with mesh size

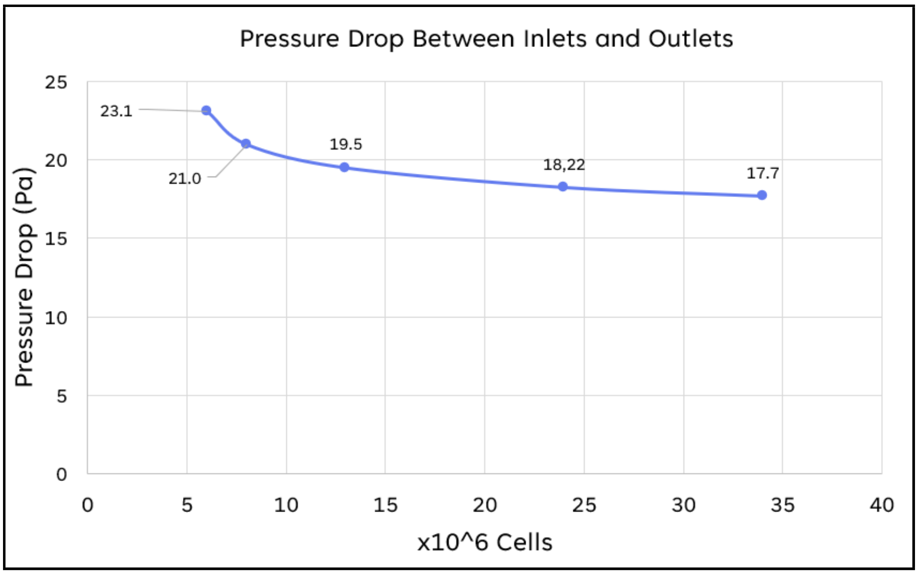

Figure 20: Variation of pressure drop with mesh size

3.5 Parametric Study

The different boundary conditions can be visualized in the table 6, and a summary of the different boundary conditions and their values can be seen in the table below. These baselines served as controlled references for subsequent localized heating configurations without altering the general boundary-condition framework.

A parametric study was conducted to evaluate the sensitivity of occupant thermal comfort to varying operational and environmental conditions. All simulations in this matrix were performed using steady-state convergence criteria to identify the final stabilized thermal environment. Four primary parameters were investigated:

- **Inlet Temperature:** The vane inlet temperature was varied between 22 °C and 36 °C to determine the optimal threshold for occupant comfort.
- **Mass Flow Rate:** Three distinct flow regimes (0.1 kg/s, 0.2 kg/s, 0.4 kg/s) were compared.
- **Occupant Presence:** Simulations were run for both "Driver Only" and "Driver + Passenger" configurations to account for the additional metabolic heat load and its impact on cabin air temperature.
- **Solar Loads:** The impact of external radiation was assessed by toggling solar flux through the glazing.

Table 6: Boundary and initial conditions used in the simulation

S. No.	Parts / Surfaces	Boundary / Initial Condition	Value / Property
1	Inlet vanes	Mass flow inlet	$0.04\,\mathrm{kg\,s^{-1}}$
2	Inlet vanes	Temperature	22 °C, 24 °C, 26 °C, 28 °C, 30 °C, 32 °C, 34 °C, 36 °C
3	Outlet vanes	Pressure outlet	1 atm
4	Floor, exterior, roof, and windows	Static ambient temperature	10 °C
5	All interior surfaces and manikins (if thermal comfort not computed)	Static temperature	16 °C
6	Driver and passenger (if thermal comfort computed)	Adiabatic	Skin temperature: 34 °C

The cold flow simulation served as a basis for the subsequent parametric study. Hence, in order to translate the same base to the parametric study, additional solvers have to be selected, which are as follows:

Table 7: Physics solvers and models enabled for the cold flow simulation

Category	**Selected Model**
Material	Gas (Ideal gas)
Flow, solver	Coupled flow (exchanged for segregated flow)
Viscous regime	Turbulent
Turbulence model	Realizable k–ε (two-layer, all y^+)
Time domain	Steady
Dimensionality	Three-dimensional
Energy loads	Coupled energy, radiation
Radiation	Surface-to-surface radiation
Radiation spectrum	Gray thermal radiation
Solar radiation	Solar loads
External forces	Gravity

It can be observed that a segregated flow solver was used for the cold flow analysis, whereas a coupled flow solver is utilized for the parametric study. The primary difference between these solvers lies in how the momentum and pressure equations are handled; the segregated solver is computationally simpler and more efficient, while the coupled solver is more resource-intensive but better suited for flows with strong fluid interactions.

Besides other solvers, other significant inclusions in the parametric study are the coupled energy, solar loads, gray thermal radiation, and surface-to-surface (S2S) radiation models, which are explained briefly in the upcoming subsections.

Inlet Temperature Study

The investigation focused on the vane inlet temperature. By sweeping the temperature from 22 °C to 36 °C, the goal was to identify the "critical temperature" required to bring the PPD below 10% for the driver. This study was performed for both male and female drivers to highlight physiological differences in heating requirements.

Mass Flow Sensitivity Study

To evaluate the trade-off between convective heating power and draft risk, the ventilation intensity was varied while keeping the inlet temperature constant. The objective was to determine if increasing or decreasing the mass flow improves the overall warming rate or detrimentally affects local comfort by increasing the convective cooling coefficient on exposed skin segments (face and hands). Two additional total mass flow rates were simulated and compared with the values from the previous subsection.

- **Low Flow (0.1 kg/s):** Minimizing air velocity to reduce draft.
- **Medium Flow (0.2 kg/s):** The baseline operational condition (for which we have the PPD value from the previous subsection)
- **High Flow (0.4 kg/s):** Maximizing convective heat delivery.

This parameter was tested exclusively on the male driver, with a specific emphasis on the PPD index. Simulations were performed to calculate the resulting PPD indices; to better understand their significance, the absolute change in PPD value relative to the baseline was utilized for analysis.

Solar Load Impact

For this study, the Solar load model in STAR-CCM+ was deactivated. The primary objective was to evaluate the impact on local thermal comfort. By analyzing the Berkeley sensation scores on specific body segments, the study assessed how asymmetric radiative heating influenced perceived comfort compared to the baseline case where the solar loads were off.

Distinction in thermal comfort of driver and passenger

This case assessed the thermal impact of introducing a second occupant. Simulations compared the baseline "Driver Only" scenario against a "Driver + Passenger" configuration, specifically focusing on the front passenger seat. All combinations of male and female occupants were simulated. Comfort indices were extracted for both occupants. Two simulation cases were performed

- Case 1: Male driver + Female passenger
- Case 2: Female driver + Male passenger

The other physical and mesh parameters for the simulation were kept the same.

3.6 Post Processing and Data Analysis

To ensure data consistency, the extraction of results was automated using Java macros.

- **Virtual Probes:** Spherical probe points (r=0.05 m) were created at critical anatomical locations: Head, Chest, Knees, and Feet, as shown in Figure 21. These probes recorded the local air temperature and velocity surrounding the occupant.
- **Volume Averages:** The volume-averaged temperature of the entire cabin fluid region was monitored to judge global convergence.

- **Comfort Indices:** The thermal comfort and the thermal sensation from 19 segments, PPD, and DTS values were extracted directly from the manikin boundaries.

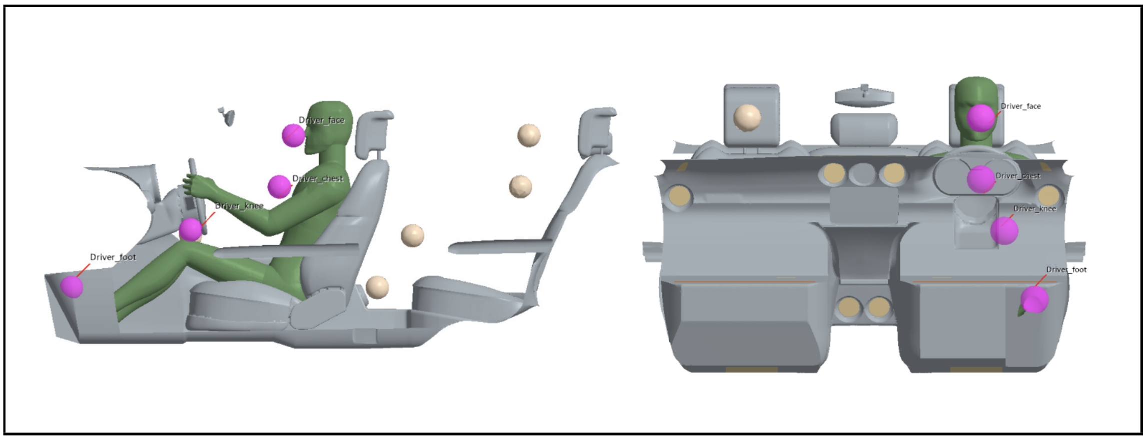

Figure 21: Position of probes at the driver's chest, face, feet, and knees

4 Results and discussions

4.1 Parametric Study

This subsection presents the results of the parametric study conducted to evaluate the sensitivity of occupant thermal comfort to variations in inlet temperature, ventilation mass flow rate, occupant presence, and solar radiation. All simulations were performed using the baseline medium mesh identified in the mesh independence study and steady state convergence criteria.

4.1.1 Inlet Temperature Sensitivity

The inlet temperature was varied from 22 °C to 36 °C in increments of 2 °C to identify the temperature range that provides acceptable thermal comfort for both male and female drivers. Thermal comfort was evaluated using the PMV and PPD indices.

The relationship between the vane inlet temperature and the average cabin temperature for both occupants is detailed in Table 8. A distinct linear relationship is observed for both cases, where increasing the inlet temperature results in a proportional rise in the average cabin temperature.

Table 8: Relationship between Inlet Temperature and Average Cabin Temperature for Male and Female Drivers

Inlet Temp (°C)	**Avg. Cabin Temp – Male (°C)**	**Avg. Cabin Temp – Female (°C)**
22	19.0	19.0
24	20.2	20.2
26	21.3	21.2
28	22.5	22.4
30	23.6	23.5
32	24.7	24.6
34	25.8	25.7
36	27.0	26.7

The correctness of the simulations can be proved by plotting a graph of dynamic thermal sensation (DTS) against the PPD for various average cabin temperature as shown in **??**. The relationship between ambient temperature and occupant comfort mirrors the PPD index. As temperatures deviate from the thermal neutral setpoint in either direction, the rate of dissatisfaction increases asymptotically, forming a parabolic distribution with the peak efficiency clustered around a specific optimal range.

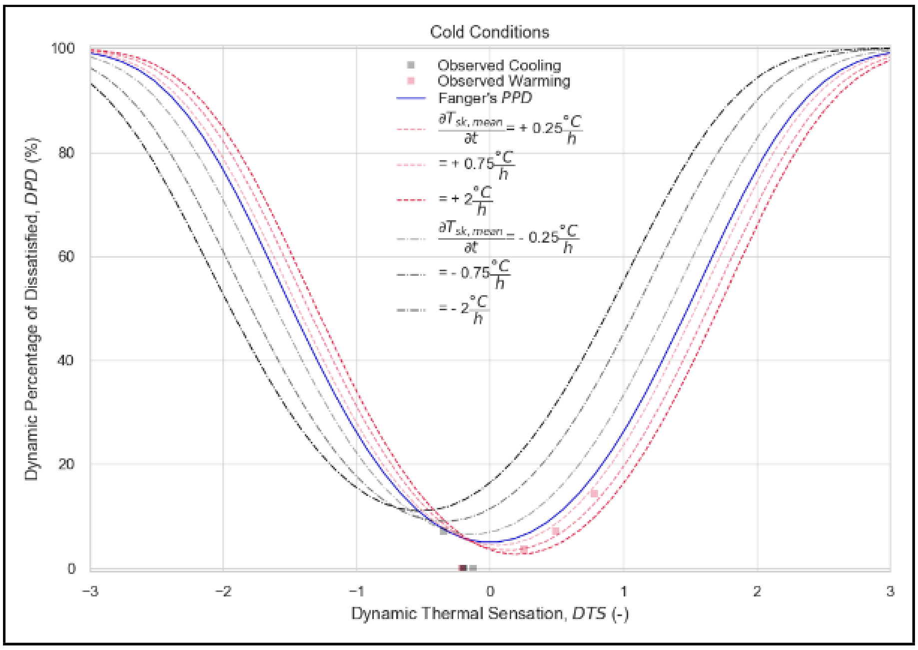

Figure 22: Fanger's DTS vs PPD relation [13]

For the male driver, the PPD index curve, which identifies the optimal temperature range for thermal comfort, is presented in Figure 23. Specifically, a minimum predicted dissatisfaction of 5% was identified when the average cabin temperature reached 24.7 °C, which corresponds to an inlet temperature of 32 °C. Since the average cabin temperatures for our cases didn't initially satisfy the right side of the inverted bell curve,e two additional extreme vane inlet temperatures corresponding to cabin average temperatures of 34.5 °C and 37.8 °Cwhich does not contribute to the other parts of the study, were simulated just to prove the relationship between DTS and PPD.

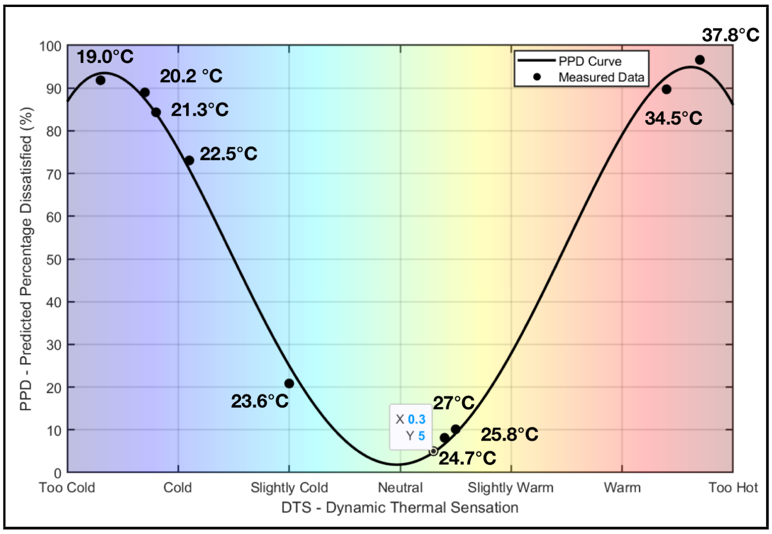

Figure 23: PPD Index Curve (Male Driver)

The same procedure was applied to the female driver configuration. As indicated in Table 8, the linear temperature trend remains consistent. The PPD index curve for the female driver is illustrated in Figure 24. Similarly, a minimum dissatisfaction of approximately 5.73% was recorded at an average cabin temperature of 24.6 °C, which was also achieved at an inlet temperature of 32 °C.

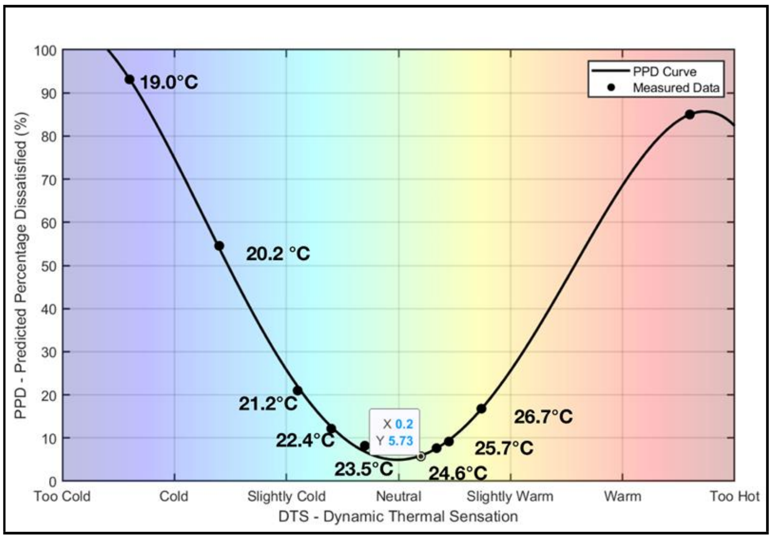

Figure 24: PPD Index Curve (Female Driver)

For both drivers, increasing the inlet temperature resulted in a reduction in dissatisfaction up to a specific minimum, followed by an increase in dissatisfaction at higher temperatures. These results suggest that an inlet temperature of 32 °C represents an optimal setpoint for minimizing aggregate dissatisfaction under the simulated conditions. A more detailed analysis of the local thermal comfort and sensation for both the male and female occupants is presented in the subsequent subsections.

Male comfort

The Berkeley local thermal comfort results for the male driver indicate a distinct occupant satisfaction. The highest comfort levels were consistently recorded in the upper body segments, specifically the chest, back, and upper arms. At an inlet temperature of 32 °C (cabin average temperature of 24.7 °C), these regions remained within the "Comfortable" to "Slightly Comfortable" range.

The higher comfort levels observed in these body segments can be attributed to a combination of elevated local skin temperatures, clothing insulation, and reduced convective heat loss. The chest and upper arm segments exhibited the highest comfort levels, driven by elevated local skin temperatures near the body's core and the significant thermal resistance provided by clothing insulation. Similarly, the back maintained a favorable thermal state due to the protective insulation of clothing and its orientation on the leeward side of the airflow, which reduces convective heat loss. Furthermore, the back benefited from the additional conductive insulation and shielding provided by the seat backrest.

A conclusion can be drawn from the figure 25a that the segments which are shielded and in contact with the seat, eg, upper body, pelvis region, and thigh area, are in the comfortable range of the spectrum due to additional conductive insulation. In contrast, the other regions,s which are actually in a stretched out position, exhibited the lowest comfort scores. Even at this optimal inlet temperature, the forearms, legs,s and feet consistently registered as "Uncomfortable" or "Slightly Uncomfortable," highlighting convective loss of heat and the challenge of delivering adequate heat to the footwell in this configuration.

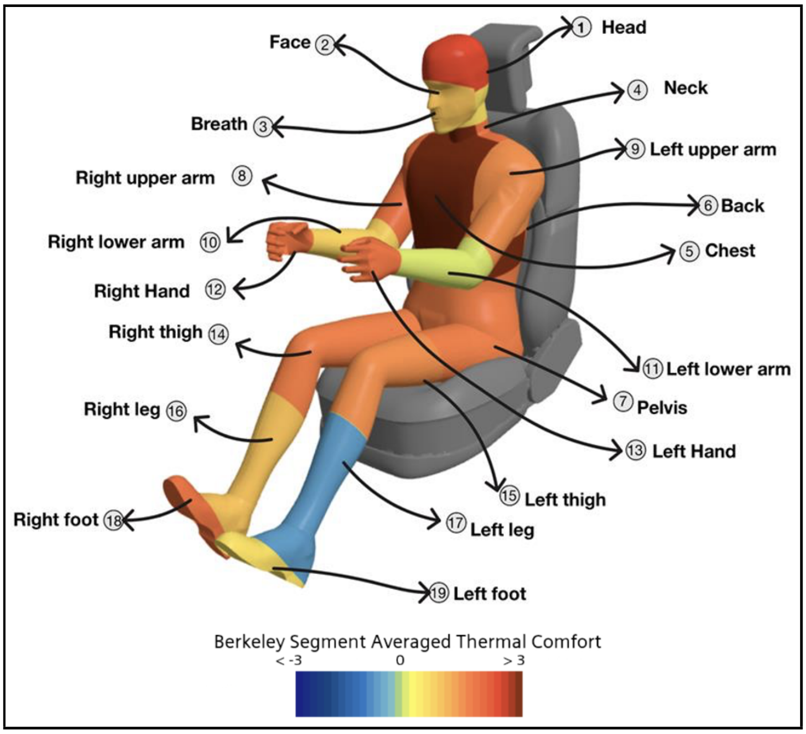

(a) Berkeley model segments

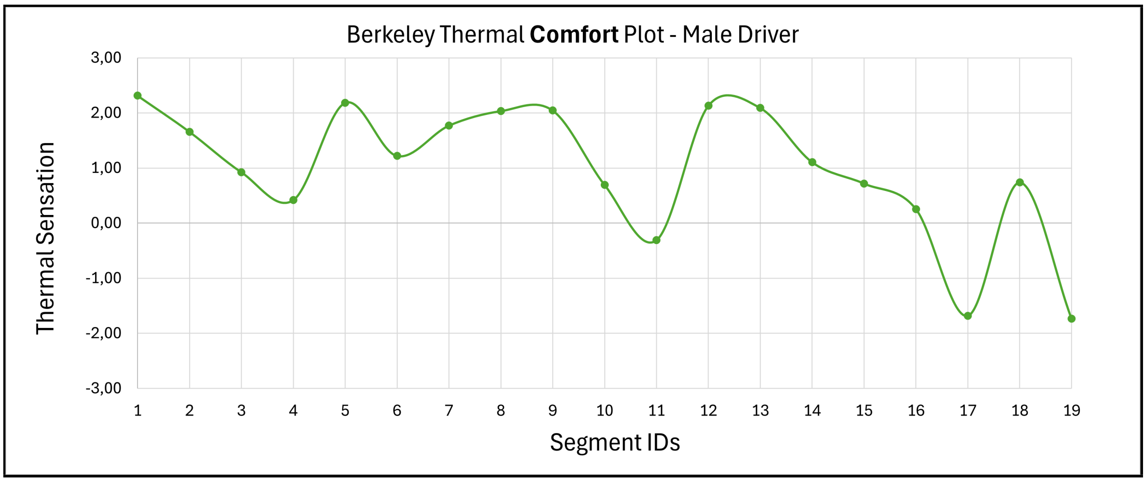

(b) Local thermal comfort distribution

Figure 25: Analysis of the male driver using the Berkeley model: (a) definition of body segments, and (b) resulting local thermal comfort distribution at 24.7 °C cabin temperature

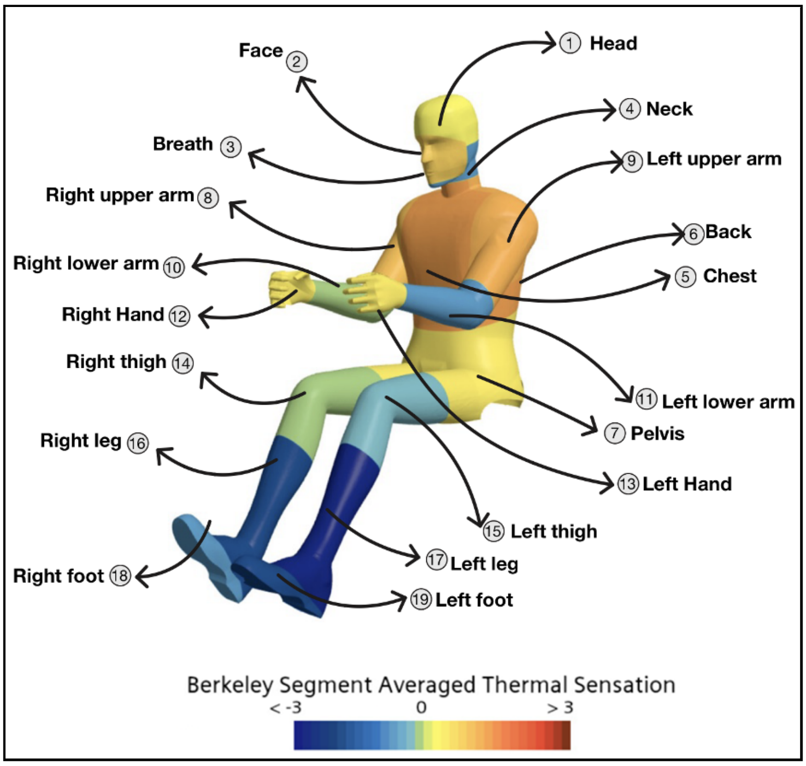

(a) Berkeley model segments

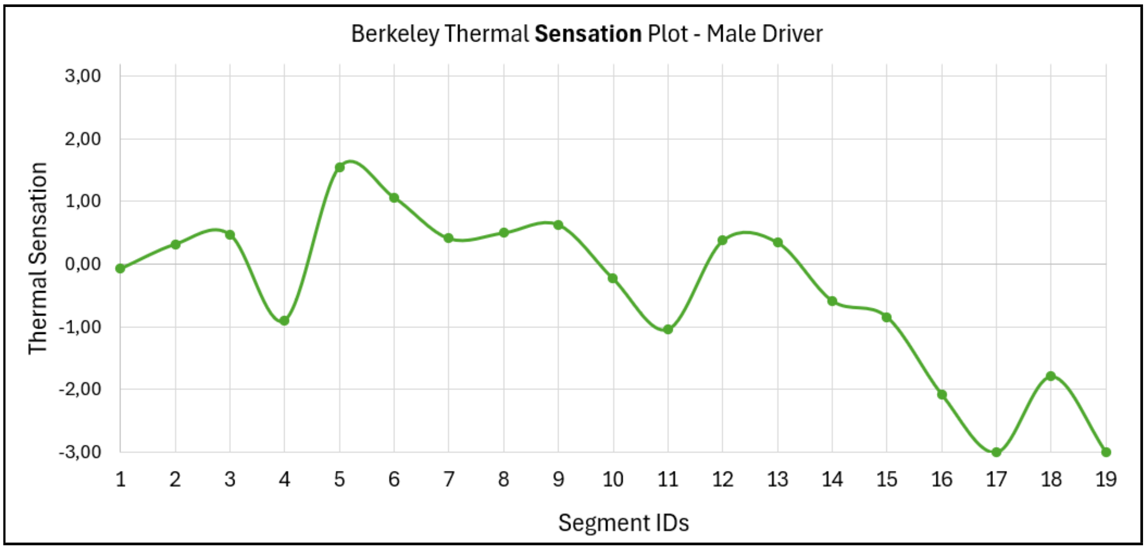

(b) Local thermal sensation distribution

Figure 26: Analysis of the male driver using the Berkeley model: (a) definition of body segments, and (b) resulting local thermal sensation distribution at 24.7 °C cabin temperature

The local thermal sensation results at 24.7 °C provide further insight into this distribution. While the head and chest regions approached a neutral sensation, a significant lateral asymmetry was observed. The segments on the driver's left side, specifically the left upper arm, left thigh, and left foot, indicated a noticeably cooler sensation compared to their counterparts on the right side.

This left-side cooling is attributed to the driver's positioning within the cabin. As the driver is seated on the outboard side, the left limbs are directly adjacent to the door and window panels. These surfaces are exposed to the external ambient temperature of 10 °C, making them significantly colder than the interior center console. Consequently, the driver experiences increased radiative heat loss from the left side of the body to these cold surfaces, creating a localized "cold wall" effect that is not present on the inboard (right) side, which, on the contrary, along with radiation, is also directly exposed to air flow from the center vents.

Female comfort

The Berkeley local thermal comfort results for the female driver exhibited a spatial distribution comparable to the male case. At the recorded comfortable cabin inlet temperature of 32 °C, leading to a cabin average temperature of 24.6 °C, homogeneous with male comfort, the highest comfort levels were recorded in the chest, back, and upper arm segments.

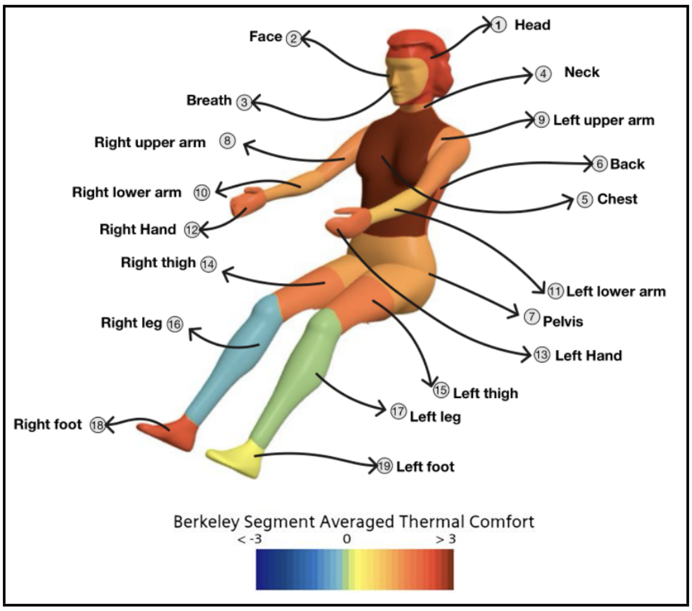

(a) Berkeley model segments

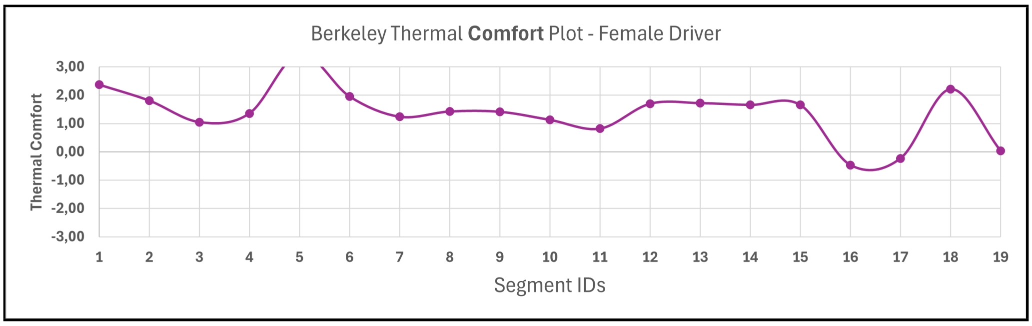

(b) Local thermal comfort distribution

Figure 27: Analysis of the female driver: (a) definition of body segments, and (b) resulting local thermal sensation distribution at 24.6 °C cabin temperature

The local thermal sensation results reveal a distinct thermal disparity at a cabin temperature of 24.6 °C. While the upper body, comprising the head, torso, and arms (Segments 1 to 13), maintained a thermally neutral state with no significant warm or cold sensation, the lower extremities experienced a marked reduction in thermal sensation. Specifically, legs and feet (Segments 16 to 19) were noticeably cold, remaining the primary regions of local discomfort due to persistent cold sensations.

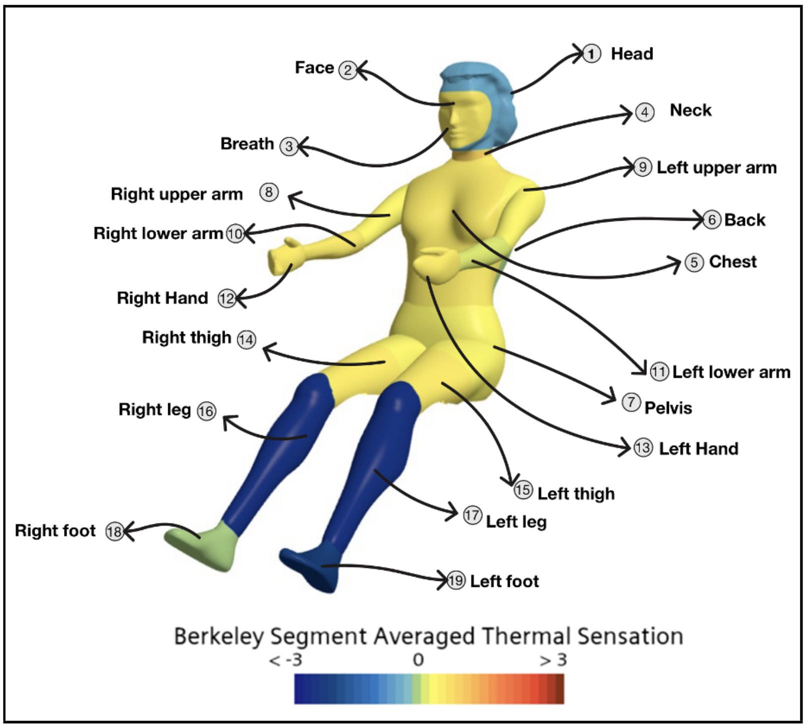

(a) Berkeley model segments

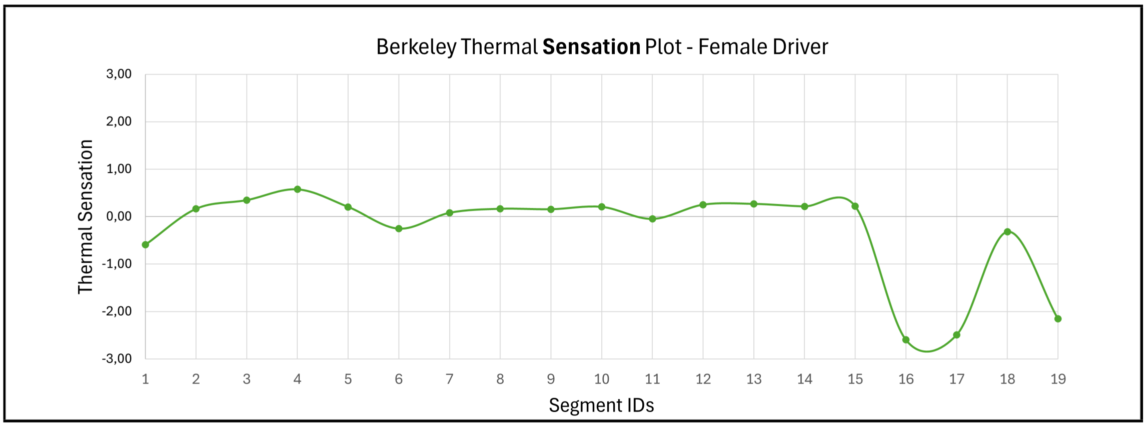

(b) Local thermal sensation distribution

Figure 28: Analysis of the female driver: (a) definition of body segments, and (b) resulting local thermal sensation distribution at 24.6 °C cabin temperature

4.1.2 Comparison of Male and Female Thermal Comfort and Sensation

A direct comparison between male and female drivers was performed at the optimal inlet temperature of 32 °C to evaluate differences in local thermal comfort and thermal sensation. The analysis focuses on identifying whether both occupants respond similarly under identical cabin conditions.

Figure 29 shows the local thermal comfort distributions for both drivers. Overall, both occupants exhibit similar comfort levels in the upper body segments (Segments 5, 6, 8, and 9), which correspond to the chest, back, and upper arms, respectively. However, a distinct divergence is observed in the lower body. The male driver shows significantly reduced comfort in the legs and feet (Segments 16-19), dipping into the uncomfortable range, while the female driver maintains a neutral to slightly comfortable state in these same regions.

To investigate the root cause of this discrepancy, the local thermal sensation results were analyzed (Figure 30). In contrast to the comfort scores, the sensation plot reveals that *both* the male and female drivers experience "cold" or "slightly cold" sensations in the legs and feet.

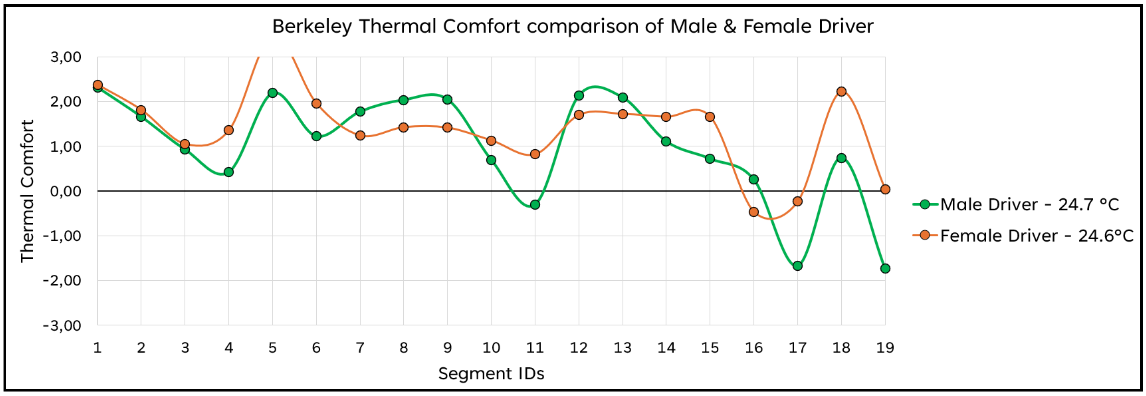

Figure 29: Comparison of local thermal comfort distribution for male and female drivers at the optimal inlet temperature

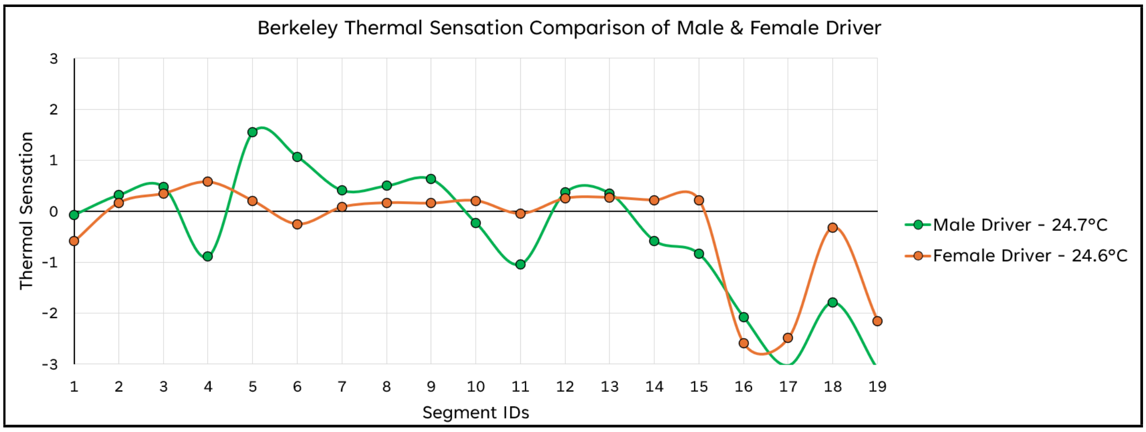

Figure 30: Comparison of local thermal sensation distribution for male and female drivers at the optimal inlet temperature

The fact that the female driver reports higher comfort despite perceiving the same cold sensation can be attributed to the physiological setpoints defined in the simulation model. As detailed in Table 2, the female manikin is assigned a lower target mean skin temperature (33.0 °C) compared to the male (34 °C). In the cooler environment of the footwell, the local skin temperature of the male manikin drops significantly below his higher target setpoint, resulting in a large error term in the comfort equation. Conversely, because the female target is set lower, her physiological state in the cool footwell aligns more closely with her defined neutral condition. The Berkeley model, therefore, interprets this smaller deviation as a higher level of thermal comfort, even though the absolute sensation is cool.

4.1.3 Mass Flow Rate Sensitivity

The influence of ventilation mass flow rate was evaluated by comparing three cases at a constant inlet temperature of 32 °C. The baseline case used a total mass flow rate of 0.2 kg/s, while additional cases of 0.1 kg/s and 0.4 kg/s were simulated.

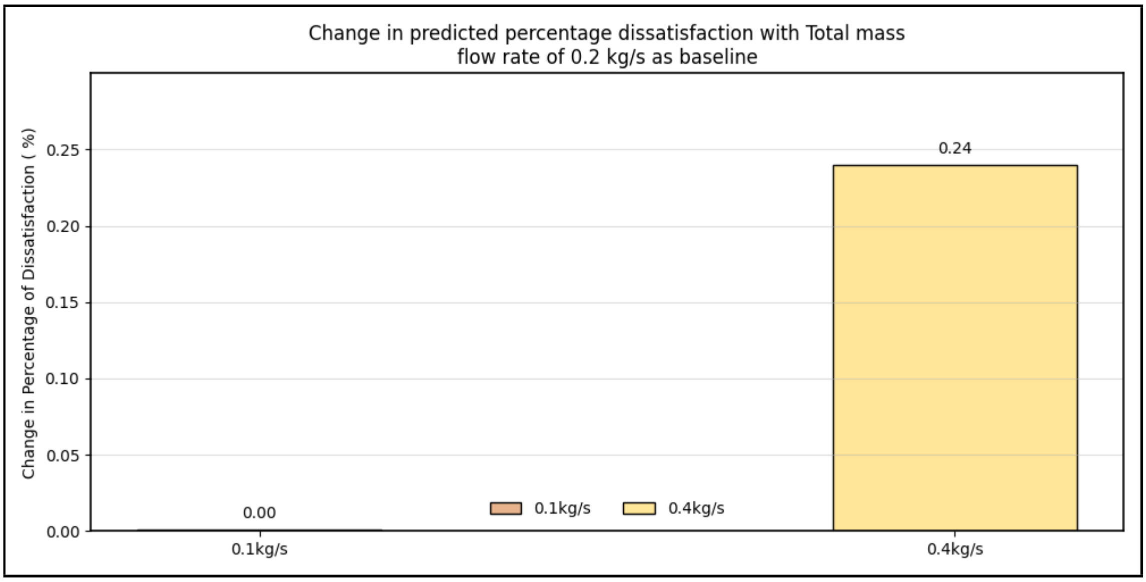

Figure 31: Impact of mass flow rate deviations on occupant dissatisfaction levels (Baseline: 0.2 kg/s)

The results demonstrate that the thermal indices are relatively robust to fluctuations in mass flow rate, considering the setup was simulated with steady state boundary conditions. Although significant deviations of -50 % and +100 % from the baseline flow (0.2 kg/s) were tested, the resulting change in predicted dissatisfaction remained within a very narrow range of $\Delta < 0.3$. The results indicate that Predicted Percentage Dissatisfied (PPD) remains relatively insensitive to decreases in mass flow rate, yet shows a marginal increase when the flow is doubled. Compared to the baseline PPD of 5.0001%, a 50% reduction in flow yielded a negligible change to 5.001%, whereas a 100% increase resulted in a PPD of 5.24%. Given that the theoretical minimum for PPD is 5% and the observed variances at lower flow rates fall within a margin of numerical insignificance for this study, we assume no practical change in comfort during flow reduction. However, doubling the mass flow rate adversely impacts comfort due to the "draft effect," where increased air velocity accelerates convective heat loss from the skin. This localized cooling effect, even at a constant cabin average temperature, heightens occupant dissatisfaction as the air movement transitions from a neutral state to a physically intrusive draft. This can be better understood.t This suggests that the system is relatively insensitive to flow rate adjustments alone when the vane inlet temperature is kept constant.

Consequently, adjusting the mass flow rate in isolation may not be an effective strategy for significantly influencing occupant thermal comfort. While these minor shifts in the tenths or hundredths of the PPD index are negligible for comfort, the negligible change in the PPD index due to the assumptions, its limitations, and the impact of mass flow adjustments on energy consumption will be discussed in further detail in the following discussion section.

4.1.4 Occupant Presence and Interaction

From Section 4.1.1, it was concluded that a vane inlet temperature of 32 °C, which corresponds to a cabin temperature of ≈ 24 °C, is the most optimal state for male and female comfort. In this subsection, the distinction between the two cases described in 3.5 is made. The thermal sensation and thermal comfort from the simulation with the passengers are represented in the figures 32 and 33.

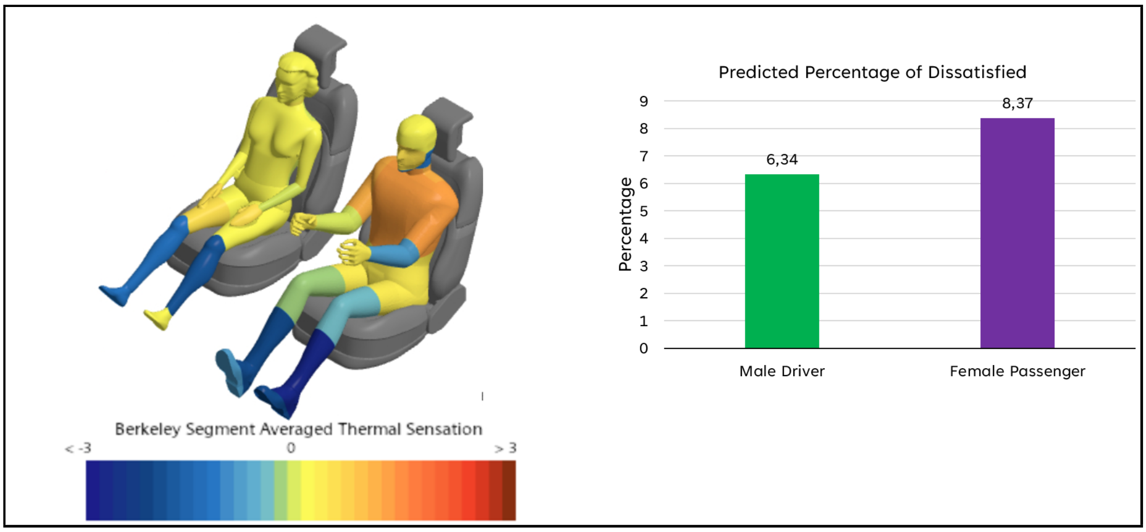

Figure 32: Berkeley averaged thermal sensation and PPD of male driver with female passenger at vane inlet temperature of 32 °C

While the visual representation of sensation suggests minimal variance between the two scenarios, a more granular analysis of the absolute values reveals distinct differences. Although both the driver and passenger remain within the range of thermal neutrality, the underlying dynamic thermal sensation indices provide a clearer differentiation of the occupant states. These quantitative values are detailed in table 9. The highlighted values (a deviation of more than 10% from each other) clearly demonstrate a distinction that the manikin model failed to capture, despite identical geometric orientation and spatial positioning within the cabin.

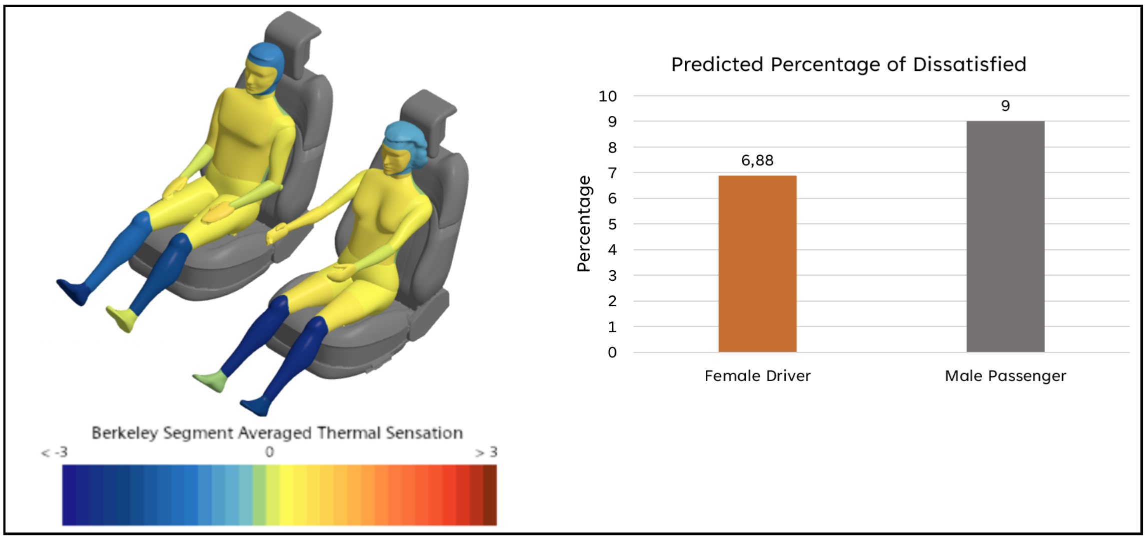

Figure 33: Berkeley averaged thermal sensation and PPD of female driver with male passenger at cabin temperature of 24 °C

Table 9: Thermal sensation comparison for driver and passenger

Segment ID	**Thermal Sensation**			
	Case 1 Driver (male)	**Case 2 Driver (female)**	**Case 1 Passenger (female)**	**Case 2 Passenger (male)**
1	**0.12**	**-0.57**	**0.03**	**-0.94**
2	0.16	0.16	0.10	0.17
3	0.49	0.41	**0.07**	**0.31**
4	**-1.20**	**0.54**	**0.24**	**0.05**
5	**1.30**	**0.20**	**0.02**	**0.21**
6	**1.04**	**-0.24**	**-0.13**	**-0.29**
7	**0.27**	**0.09**	0.11	0.16
8	**1.01**	**0.15**	0.14	0.21
9	**1.12**	**0.15**	0.13	0.13
10	**-0.04**	**0.20**	**0.10**	**-0.04**
11	**-0.90**	**-0.04**	-0.15	-0.08
12	0.25	0.24	0.45	0.37
13	0.26	0.26	0.38	0.42
14	**-0.20**	**0.21**	**0.43**	**0.16**
15	**-0.42**	**0.21**	0.13	0.18
16	**-1.93**	**-2.56**	-1.28	-1.45
17	**-2.67**	**-2.47**	**-1.81**	**-2.01**
18	**-0.91**	**-0.29**	**-1.20**	**-2.33**
19	**-1.87**	**-2.12**	0.08	-0.01

The qualitative color mapping suggests a thermal gradient between the cranial and facial regions of case 2, characterizing the former as "cool" and the latter as "neutral". The quantitative data in the associated plots do not support a statistically significant distinction. On the other hand, the localized analysis of the lower extremities reveals that the inner feet maintain higher comfort levels relative to the outer feet. This spatial variance is attributed to the specific arrangement of the HVAC system, where the primary vents are positioned directly above the interior footwell. The outer feet and the outer upper arm of the driver also experience a relative cold sensation due to the fact that they are positioned next to a convective boundary, which is exposed to an ambient temperature of 10 °C. Due to a shortage of air circulation near the lower leg area of the occupants in the front and due to the short circuit of the inlet air, discussed in the section 3.3, the lower leg segments are relatively colder and, in turn, relatively more uncomfortable, irrespective of the occupant position in the front.

An evaluation of PPD metrics initially suggests that gender-based physiological differences are negligible. While gender exerts a secondary influence on thermal state via metabolic activity rates and skin temperature, the dominant driver of thermal comfort in this study is the occupant's spatial position within the cabin. Both male and female drivers consistently exhibited lower PPD values compared to passengers, regardless of gender-specific physiological inputs.

The superior comfort profile of the driver is primarily a function of cabin geometry and airflow distribution. The driver's position facilitates more effective convective cooling across the upper body while simultaneously maintaining thermal equilibrium in the lower body. This balanced distribution effectively minimizes the temperature gradients between body segments, a critical factor in the calculation of PPD, thereby resulting in a more favorable overall thermal sensation than that experienced by the passenger.

4.1.5 Solar Load Impact

The impact of solar radiation was evaluated by comparing a baseline condition, which is the case with the most optimal comfort state from the initial parametric study, with a case excluding the active solar loads. The exclusion of the solar loads can - to an extent - be intuitively understood on a cloudy day, evenings, or even in tunnels.

In STAR-CCM+, the solar load model applies realistic heating to the CFD domain by utilizing a ray-tracing algorithm that projects rays - spanning the ultraviolet, infrared, and visible spectrum - from a defined solar source onto target surfaces. While the gray thermal radiation model accounts for surface emissivity and absorptivity, the S2S model works in conjunction with these solar loads to compute the subsequent radiative heat exchange between internal surfaces. The solver determines energy distribution based on geometric orientation and boundary-level properties, distinguishing between opaque surfaces that reflect or absorb energy and Semi-Transparent surfaces, like glass, that allow radiation to pass through based on defined transmissivity. By automatically accounting for shadowing and direct line-of-sight, this integrated approach accurately computes localized heat fluxes, which are essential for evaluating occupant thermal comfort and sensation.

From the figure 34, a few conclusions can be drawn. The presence of solar radiation resulted in higher local thermal comfort and sensation values on the window-facing side of the driver. With the solar loads and radiation switched off, the

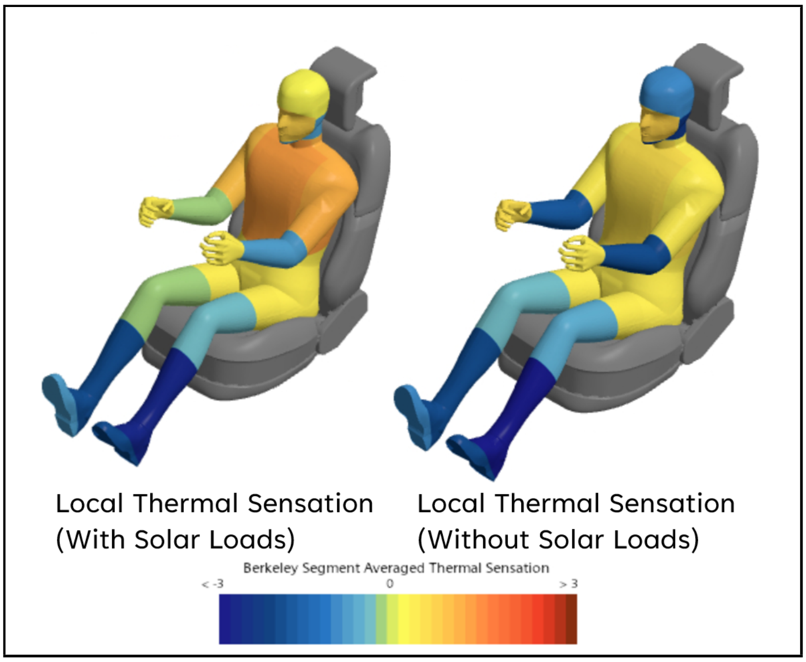

Figure 34: Comparison of driver thermal sensation with and without solar and radiation loads

dashboard and interior of the cabin, which are exposed to the radiation reaches a relatively colder temperature andmatchs the cabin average temperature of 24 °C. Hence, the only heat the passenger receives is from the inlet vane. Since the human body loses heat to its surroundings for the same cabin temperature of 24 °C with the relatively colder interior surfaces, the occupants (in this case, the driver) feel "chilly". This could also mean that the occupants will feel relatively cold at 24 °C at night, in tunnels, or on a cloudy day.

Because the PPD is highly sensitive to local radiant heat and surface temperature differences, not just average air temperatures, body segments exposed to solar radiation exhibited warmer thermal sensation compared to the shaded side. Overall comfort distributions differed noticeably between the two cases, with the dynamic thermal sensation shifting from ≈ 0.3 (slightly above neutral) to ≈ 2 (cold), highlighting the importance of solar and radiation loads on passenger comfort.

5 Conclusion and Future scope

An average cabin temperature of ≈ 24.6 °C provided the highest thermal comfort for both male and femaledriversr

Based on the initial parametric study of inlet vane temperatures, a cabin average of 24.6 °C (derived from a 32 °C inlet temperature) was identified as the optimal thermal setpoint for both male and female occupants. While physiological data indicated localized variations in comfort preferences between male and female models at specific body segments, the PPD values remained consistently low under the investigated conditions. Specifically, at an average temperature of approximately 24.6 °C, the PPD reached its minimum, indicating a dissatisfaction rate of nearly 5 % for both genders.

Changes in inlet mass flow rate had a limited impact on comfort when steady state is considered, but still have potential for energy savings in transient conditions

The mass flow rate of an HVAC system brings little to negligible changes in the dissatisfaction of occupants. This could be primarily due to the assumptions made for this study. The study was performed using steady-state boundary conditions. Since the cabin reaches a thermal equilibrium, increasing or decreasing the mass flow rate does not contribute much to the results.

Nevertheless, in a transient environment, mass flow rate could play a role in comfort, where recirculation and temporal dependency to reach a set cabin temperature are of major importance. In a BEV operating in extreme cold, the total HVAC system power demand can reach 5 kW to 10 kW, depending on the use of resistive PTC heaters or heat pumps. However, the blower motor alone is a relatively minor contributor, typically consuming between 200 W and 600 W (0.2–0.6 kW) to circulate air throughout the cabin. With an initial baseline of 0.2 kg/s at an assumed typical power draw of 300 W, Table 10 shows how the consumption scales when you change the mass flow rate:

Table 10: Effect of different mass flow rates on the energy consumption of the battery with 0.2 kg/s as the baseline

Total Mass Flow Rate $\dot{m}$ (kg/s)	**Power Consumption P (W) ≈ estimated**
0.1	≈ 37.5 – 50
0.2	300
0.4	≈ 2100 – 2400

One can see how the power consumption increases cubically, based on fan affinity laws, assuming constant air density and similar blower efficiency across operating points. In the long run, reducing the mass flow rate to 0.1 kg/s (half of the 0.2 kg/s baseline) offers a marginal but measurable advantage for vehicle range. Compared to the 0.2 kg/s baseline (approx. 300 W), a savings of roughly 250 W of continuous draw. Over a 4-hour winter highway drive, this preserves about 1 kWh of battery capacity - equivalent to roughly 3–5 km of additional range.

Solar loads have a strong influence on the internal cabin temperature and must be included for realistic PPD predictions

In the presence of solar loads, a lower interior temperature setpoint is preferable as radiant heat provides a natural baseline for occupant comfort. Relying solely on ambient temperature sensors often leads to over-conditioning of the cabin air. Instead, HVAC systems could integrate pyranometers or dedicated solar load sensors to quantify real-time radiant energy and dynamically adjust the cabin temperature. This transition from a constant setpoint to a radiation-aware control logic optimizes thermal sensation while significantly reducing battery energy consumption.

Localized heating, on the contrary to centralized heating, leads to a power saving

Transitioning from a centralized cabin climate control system to a localized heating architecture offers a more efficient pathway for achieving optimal occupant comfort. While centralized systems must condition the entire cabin volume, localized solutions target the specific thermal needs of the passengers, thereby maintaining comfort levels while significantly reducing the energy burden on the vehicle's battery. According to Chen et al. [14], localized thermoelectric (TE) cooling and heating systems can significantly enhance the energy efficiency of electric vehicles by focusing thermal conditioning on specific occupant body areas rather than the entire cabin. By integrating TE modules for the face, chest, lap, and feet, along with a high-efficiency contact TE seat, researchers established equivalent thermal comfort to a baseline HVAC system while achieving annualized energy savings of 37.7 % for heating and 36.7 % for cooling. Chen's study validated these findings using human subject road tests and objective thermal manikin measurements to ensure that the reduced power consumption did not compromise passenger comfort.

Implementation of a proprietary thermo-physiological model for female and other occupant positions is recommended to capture gender-specific thermal comfort thresholds

The male passenger, female driver, and female passenger were not the same as those of the male driver modeled by the STAR-CCM+. Since the CAD models were manipulated and the segmentation was done manually, and does not correspond to the same segments as of the ones provided, the mathematical computation could lead to some discrepancies, for example the thermal comfort of female driver at segment 5 (Chest) was more than 3, which is not possible in a mathematical model with spectrum from -3 to +3. The presence of cold sensation without corresponding discomfort for the female driver suggests a limitation of the Berkeley thermal comfort model used in STAR-CCM+. The model is unisex with fixed height and weight properties and applies the same comfort interpretation to both occupants. As a result, local discomfort in peripheral regions for female occupants may be underestimated. This, therefore, necessitates the development of a proprietary female-specific mathematical model within STAR-CCM+ to enable a more accurate assessment of female thermal comfort.

Proper insulation allows comfortable conditions at lower cabin temperatures, reducing HVAC energy demand

Enhancing cabin insulation represents a strategic alternative for optimizing passenger thermal comfort. By mitigating parasitic heat transfer, this approach conserves energy delivered by the HVAC system and extends the residence time of thermal energy within the cabin environment. As analyzed and verified by Ramesh Babu et al [15], a vehicle driving at 50 km/h in -7 °C conditions and fully insulated cabin reaches a desired 20 °C temperature in just 7.5 minutes compared to 23 minutes for a non-insulated baseline, resulting in a mean cabin temperature increase of 5.6 °C. Among individual components, seat insulation provided the most substantial benefit, increasing the mean temperature by 2.3 °C and reducing heater energy consumption by 30.74 % due to the mitigation of parasitic heat losses to the seats' large thermal mass. The study further established an asymptotic relationship between thermal resistance and temperature rise, suggesting that a resistance of 4 m^2K/W is sufficient to achieve a 9 °C increase. These findings, validated by climatic wind tunnel experiments, provide a numerical framework for optimizing material choices to reduce auxiliary loads and extend the driving range of electric vehicles.

Effect of geometry and placement of inlet vents, climate control systems

Furthermore, optimal operating strategies can be developed to adjust cabin comfort based on individual occupant perception rather than centralized control. While the simulation results of this research suggest that male and female thermal preferences converge at the same temperature, a study by Yun et al. [16] involving 80 Korean female participants indicates that gender significantly influences thermal comfort. Their findings reveal that females generally exhibit a higher sensitivity to air temperature and a lower sensitivity to humidity compared to their male counterparts. Distinctly, women often exhibit lower mean skin temperatures and higher core temperatures than men in identical conditions, and they typically prefer "neutral to slightly warm" environments, whereas men often prefer "neutral to slightly cool" settings. Because females can experience greater thermal discomfort in the non-uniform environments of a vehicle, this model provides a specialized tool for designing customized air-conditioning systems that address these unique gender-specific needs.

Consequently, HVAC system design should incorporate occupancy-based sensing to detect the presence of female passengers and autonomously modulate climate control parameters to suit their specific thermal requirements. Furthermore, component placement remains a critical factor in performance. Experimental results indicate that localized cooling in the leg area is attributable to a pneumatic short-circuit, where a lack of airflow and heat from the front floor vents occurs because the outlet is positioned in immediate proximity to the inlet. While the current configuration increases air residence time via enhanced recirculation to the rear cabin, relocating the outlet to the rear of the vehicle would likely yield superior results in terms of overall occupant comfort.

References

[1] Walsh, P; Isaac, R; Vijayagopal, R; Rousseau, A; Seo, J; Kim, N. Impact of Cold Ambient Temperature and Extreme Conditions on Electric Vehicles

[2] AEP Cabin Comfort Proposal Volvo Cars/Chalmers, 2025.

[3] Oertel H., Böhle M., Reviol T. Strömungsmechanik für Ingenieure und Naturwissenschaftler, 7th Edition, 2015

[4] Engineering Toolbox
Retrieved January 11, 2026 from Link

[5] ISO 7730 *Ergonomics of the thermal environment - Analytical determination and interpretation of thermal comfort using calculation of the PMV and PPD indices and local thermal comfort criteria* Link

[6] Van Hoof, J. (2008), *Forty years of Fanger's model of thermal comfort: comfort for all?* Indoor Air, 18: 182-201. Link

[7] Toby Cheung, Stefano Schiavon, Thomas Parkinson, Peixian Li, Gail Brager (2019), *Analysis of the accuracy on PMV – PPD model using the ASHRAE Global* Thermal Comfort Database II, Building and Environment, 153, 205-217 Link

[8] Siemens Digital Industries Software. (2024). *STAR-CCM+ User Guide: Human Thermal Comfort Models.* Siemens PLM Documentation.

[9] International Organization for Standardization. (2007). *ISO 9920: Ergonomics of the Thermal Environment - Estimation of Thermal Insulation and Water Vapour Resistance of a Clothing Ensemble.* Link

[10] Pan, N. (2019). *Unique Thermal Properties of Clothing Materials.* Global Challenges, 3(6), 1800082. Link

[11] Khatoon, S.; Kim, M.-H. (2020). *Thermal Comfort in the Passenger Compartment Using a 3-D Numerical Analysis and Comparison with Fanger's Comfort Models.* Energies, 13(3), 690. Link

[12] Liu Yang, Shengkai Zhao, Siru Gao, Hui Zhang, Edward Arens, Yongchao Zhai. (2021). *Gender differences in metabolic rates and thermal comfort in sedentary young males and females at various temperatures* Energy and Buildings, 251, 111360.

[13] Vellei, M; Le Dréau1. *On the prediction of dynamic thermal comfort under uniform environments* Windsor Conference 2020

[14] Chen, K., Bozeman, J., Wang, M., Ghosh, D. *Energy Efficiency Impact of Localized Cooling/Heating for Electric Vehicle* SAE Technical Paper 2015-01-0352, 2015 Link

[15] Babu, R.A.; Sebben, S.; Bark, T. (2023). *Effect of Cabin Insulation on the Heating Performance in EVs at Low Temperatures.* SAE Technical Paper 2023-01-0763. Link

[16] Yun, S.; Chun, C.; Kwak, J.; Park, J.S.; Kwon, C.; Kim, S.; *et al.* (2021). *Prediction of Thermal Comfort of Female Passengers in a Vehicle Based on an Outdoor Experiment.* Energy and Buildings, 248, 111161. Link